





Arabidopsis Ca²⁺-ATPases 1, 2, and 7 in the endoplasmic reticulum contribute to growth and pollen fitness

Maryam Rahmati Ishka ^{1,†}, Elizabeth Brown,¹ Alexa Rosenberg,¹ Shawn Romanowsky,¹ James A. Davis ¹, Won-Gyu Choi ¹ and Jeffrey F. Harper ^{1,*,#}

¹ Department of Biochemistry and Molecular Biology, University of Nevada, Reno, Nevada 89557, USA

*Author for communication: jfharper@unr.edu

[†]Present address: Soil and Crop Sciences Section, School of Integrative Plant Science, Cornell University, Ithaca, NY 14853, USA.

[#]Senior author.

M.R.I. conceived and performed the experiments and wrote the manuscript; S.R. isolated knockout lines; E.B. and A.R. assisted in subcellular localization experiments; J.A.D. assisted in RT-qPCR experiments; W.C. performed Ca²⁺ imaging; J.F.H. supervised experiments and assisted in plant crosses and writing. All authors contributed constructive comments on the manuscript.

The author responsible for distribution of materials integral to the findings presented in this article in accordance with the policy described in the Instructions for Authors (<https://academic.oup.com/plphys/pages/general-instructions>) is: Jeffrey F. Harper (jfharper@unr.edu).

Abstract

Generating cellular Ca²⁺ signals requires coordinated transport activities from both Ca²⁺ influx and efflux pathways. In *Arabidopsis* (*Arabidopsis thaliana*), multiple efflux pathways exist, some of which involve Ca²⁺-pumps belonging to the Autoinhibited Ca²⁺-ATPase (ACA) family. Here, we show that ACA1, 2, and 7 localize to the endoplasmic reticulum (ER) and are important for plant growth and pollen fertility. While phenotypes for plants harboring single-gene knockouts (KOs) were weak or undetected, a triple KO of *aca1/2/7* displayed a 2.6-fold decrease in pollen transmission efficiency, whereas inheritance through female gametes was normal. The triple KO also resulted in smaller rosettes showing a high frequency of lesions. Both vegetative and reproductive phenotypes were rescued by transgenes encoding either ACA1, 2, or 7, suggesting that all three isoforms are biochemically redundant. Lesions were suppressed by expression of a transgene encoding NahG, an enzyme that degrades salicylic acid (SA). Triple KO mutants showed elevated mRNA expression for two SA-inducible marker genes, *Pathogenesis-related1* (*PR1*) and *PR2*. The *aca1/2/7* lesion phenotype was similar but less severe than SA-dependent lesions associated with a double KO of vacuolar pumps *aca4* and *11*. Imaging of Ca²⁺ dynamics triggered by blue light or the pathogen elicitor flg22 revealed that *aca1/2/7* mutants display Ca²⁺ transients with increased magnitudes and durations. Together, these results indicate that ER-localized ACAs play important roles in regulating Ca²⁺ signals, and that the loss of these pumps results in male fertility and vegetative growth deficiencies.

Introduction

Ca²⁺ signals participate in nearly all aspects of plant development, including responses to biotic and abiotic stresses. The dynamic changes in cytosolic calcium concentrations [Ca²⁺]_{cyt} result from the coordinated regulation of both

influx and efflux pathways, with different Ca²⁺ circuits functioning in various subcellular locations (Tang and Luan, 2017; Aldon et al., 2018; Kudla et al., 2018; Johnson et al., 2019; Moeder et al., 2019; García Bossi et al., 2020; Martí Ruiz et al., 2020). Potential Ca²⁺-permeable influx channels

include Two Pore calcium (TPC) channels, Cyclic Nucleotide Gated Channels, Glutamate-Like Receptors, Mechano-Sensitive-Like channels, piezo type channels (Piezo), “reduced hyperOsmolality-induced $[Ca^{2+}]_{cyt}$ increase” channels (OSCA), and annexins (Demidchik et al., 2018; Kudla et al., 2018). On the efflux side, pumps and exchangers provide energized transport to remove Ca^{2+} from the cytosol and restore basal levels of $[Ca^{2+}]_{cyt}$. These transporters include Ca^{2+} exchangers (CAXs; i.e. Ca^{2+} - H^{+} antiporters) and two classes of P-type ATPases, named endoplasmic reticulum (ER)-type Ca^{2+} -pumping ATPases (ECAs; P2A ATPases) and Autoinhibited Ca^{2+} ATPases (ACAs; P2B ATPases; Axelsen and Palmgren, 2001; Baxter et al., 2003; Pittman and Hirschi, 2016; Hocking et al., 2017; Ma and Berkowitz, 2017; García Bossi et al., 2020).

In *Arabidopsis* (*Arabidopsis thaliana*), there are at least 15 ATP-dependent pumps that transport Ca^{2+} , including 10 ACAs, 4 ECAs, and a heavy metal ATPase (HMA1) that can also transport Ca^{2+} (Moreno et al., 2008). With the exception of ACA12 and 13, ACA-type pumps are activated by Ca^{2+} /calmodulin binding to an N-terminal regulatory domain, which disrupts autoinhibition and thereby activates the pump (Demidchik et al., 2018; Kudla et al., 2018; García Bossi et al., 2020). This creates a feedback mechanism through which Ca^{2+} influx generates a “transient” (signal) which then stimulates ACA-efflux pathways to help restore $[Ca^{2+}]_{cyt}$ to resting basal levels. Ca^{2+} pumps and exchangers have been found in multiple membrane systems, including the ER, vacuole, and plasma membrane (PM). While ACAs, ECAs, and CAXs remove Ca^{2+} from the cytosol, their individual contributions in controlling the magnitude or duration of different stimulus-specific Ca^{2+} signals are not well understood.

ACAs are important for a variety of physiological processes (García Bossi et al., 2020). ACA9 is PM-localized and expressed primarily in pollen, where it plays critical roles in pollen tube growth and sperm discharge, with *aca9* knockout (KO) mutants displaying severe male fertility defects (Schjøtt et al., 2004). Mutants lacking combinations of other PM-localized ACAs (ACA8, 10, 12, and 13) have been linked to altered plant morphology (ACA8 and 10 in George et al., 2008; Zhang et al., 2014), impaired reproduction (ACA8, 10, 12, and 13 in Iwano et al., 2014; Yu et al., 2018), and deficient responses to pathogens (ACA8 and 10 in dit Frey et al., 2012). ACA4 and 11 are targeted to vacuoles (Lee et al., 2007), and double mutants lacking both pumps (*aca4/11*) display a high frequency of salicylic acid (SA)-dependent lesions in leaves, which could be suppressed by disrupting an SA-biosynthesis gene *Salicylic acid Induction Deficient2* (*SID2*), which encodes Isochorismate Synthase1 (ICS1), or by expression of an SA-degrading NahG (salicylate hydroxylase) enzyme (Boursiac et al., 2010). A disruption of the *aca4/11* vacuolar pumps increases the magnitude of Ca^{2+} signals triggered by a *flg22* elicitor (Hilleary et al., 2020). RNA interference (RNAi) silencing of *NbCA1* in *Nicotiana benthamiana*, which shares greatest similarity to

ACA4 and 11, also results in increases in the magnitude and duration of cytosolic Ca^{2+} transients following exposure to a fungal elicitor (cryptogein), and these lines display similar lesion phenotypes as *aca4/11* mutants (Zhu et al., 2010). For the subgroup of ACA1, 2, and 7 (P2B-1 subfamily in *Arabidopsis* (Baxter et al., 2003), the only KO phenotype reported is for *aca7*, which displays a high frequency of aborted pollen grains detected via Alexander staining (Lucca and León, 2012). However, this *aca7* phenotype is not corroborated with genetic transmission assays, and Alexander staining has been shown to be an unreliable marker for pollen viability (Luria et al., 2019).

In this study, we provide evidence that members in the ACA1/2/7 subgroup are functionally interchangeable and reside primarily in the ER. The loss of all three pumps (*aca1/2/7*) resulted in plants with multiple phenotypes, including pollen transmission deficiencies and SA-dependent lesions in rosette leaves. Ca^{2+} imaging in leaves indicated that *aca1/2/7* mutants display Ca^{2+} transients with increased magnitudes and duration when stimulated by blue light or *flg22*. These results establish the importance of the ER-localized ACA1/2/7 subgroup in attenuating cellular Ca^{2+} dynamics and suggest that natural or engineered variation in their activities could impact multiple features of plant growth and responses to the environment.

Results

Phylogenetic and expression analyses

Four different subgroups of ACA-type Ca^{2+} -ATPases were previously established in phylogenetic analyses of P-type ATPases, with these distinct clusters showing conservation between *Arabidopsis* and rice (*Oryza sativa*; Baxter et al., 2003; Pedersen et al., 2012). Figure 1 provides a similarity tree diagram showing four ACA subgroups and other representative P-type ATPases in *Arabidopsis*. ACA1, 2, and 7 are members of the same subgroup (P2B-1). Expression profiles archived in public databases indicate that ACA2 has significant mRNA abundance in pollen, root, and leaf tissues (Figure 1; Supplemental Table S1). In contrast, ACA7 is primarily expressed in pollen and ACA1 in root and leaves. This suggests that most tissues or cells express at least two members of this ACA group, providing an expectation for functional redundancy that could mask KO phenotypes for individual genes.

ACA1, 2, and 7 have similar endomembrane localization patterns

While ER localization has been established for ACA2 (Hong et al., 1999; Dunkley et al., 2006), a side-by-side Fluorescent Protein (FP)-tagging comparison was not previously done with ACA1 and 7 to determine if they show similar subcellular localizations. To make this comparison, transgenes encoding ACA1, 2, and 7 were engineered with a C-terminal Green Fluorescent Protein (GFP) or Yellow Fluorescent Protein (YFP) and stably expressed in vegetative tissues (Figure 2), or in pollen (Figure 3).

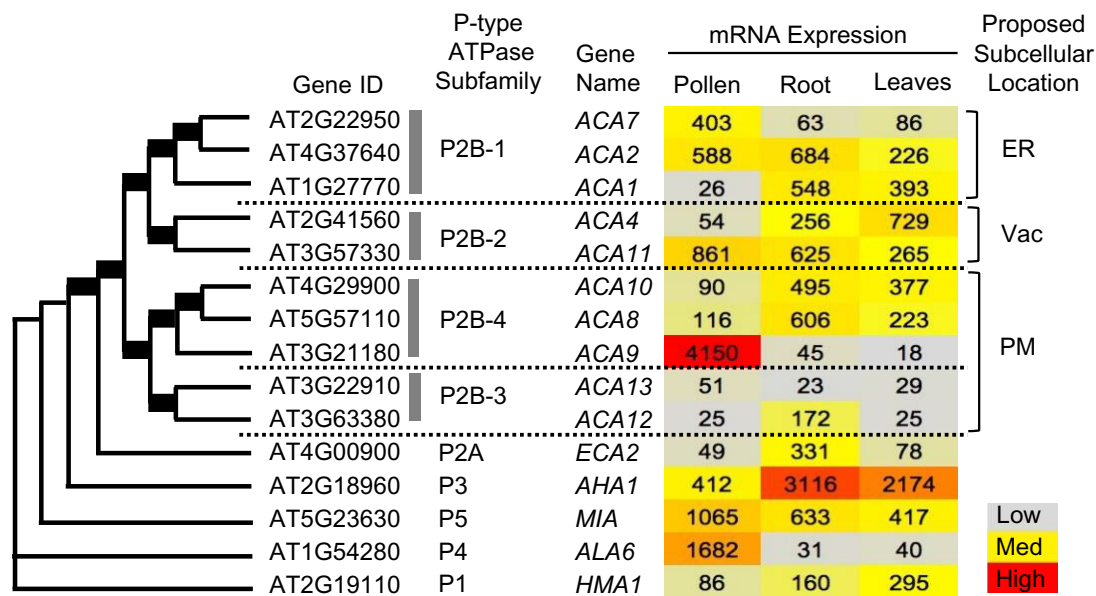


Figure 1 Similarity tree showing four distinct subfamilies of ACA-type Ca^{2+} P-type ATPases. The similarity tree was obtained from Pollen RCN (<http://arabidopsis-heat-tree.org/>) using full-length protein sequences of all 10 members of P2B ATPases with one representative member from each of the other P-type ATPases (P1, P2A, P3, P4, P5). Bold lines in tree branches indicate boot-strap values of 100. Heat map showing gene expression profiles in pollen, root, and leaves based on microarray experiments values from (<http://arabidopsis-heat-tree.org/>). A more complete expression profile comparison with all P-type ATPases is provided in [Supplemental Table S1](#), along with a comparison with two RNA-seq data sets. ER, endoplasmic reticulum; Vac, vacuole; PM, plasma membrane.

In guard cells, an ER-like pattern was observed for ACA1-YFP, ACA2-GFP, and ACA7-YFP ([Figure 2](#)). Strong fluorescence was observed surrounding the nucleus, consistent with the nuclear envelope or the ER that often “wraps” around the nucleus. These patterns were observed even in cells showing weak GFP or YFP signals near the lower limits of detection. In contrast to the PM-localized ACA8, no definitive signals corresponding with PM-localization were detected for ACA1, 2, or 7. Importantly, ACA1 did not appear to colocalize with any autofluorescence from chloroplasts, suggesting that chloroplasts are not a primary location for ACA1, in contrast to what was previously proposed by ([Huang et al., 1993](#)) based on cell fractionation and immuno-detection with a putative anti-ACA1 antibody. The lack of chloroplast co-localization was consistent among ACA1, 2, and 7.

In pollen, ER-like patterns were also observed for ACA1-YFP, ACA2-GFP, and ACA7-YFP ([Figure 3](#)). In contrast to PM-localized ACA9 ([Figure 3B](#)), ACA1, 2, or 7 did not show any significant enrichment at the PM ([Figure 3, C–E](#)). Because ACA7 was previously proposed to localize to the PM ([Lucca and León, 2012](#)), additional transgenic lines were engineered with ACA7-YFP under the control of an ACA7 promoter. Regardless of the promoter, or variations in expression levels, we did not observe any significant PM accumulation for ACA7 ([Figure 3E; Supplemental Figure S1](#)). For ACA1-YFP expressed in pollen, a higher resolution image obtained from a spinning disc confocal microscope is shown in [Supplemental Figure S1](#), with a movie ([Supplemental Movie S1](#)) that captured cytoplasmic streaming of ACA1-

labeled membranes in a pattern consistent with expectations for ER-strands. Together, these results confirm similar ER-localization patterns for the ACA1/2/7 subgroup in both vegetative and reproductive cell types.

ACA1, 2, and 7 fail to functionally replace the PM-localized ACA9

Despite the lack of PM-localization evidence for any of the ACA1/2/7 pumps, we used a genetic approach to independently determine whether any member of the ACA1/2/7 subgroup might still provide some Ca^{2+} -pumping activity at the PM. We tested whether the pollen-specific expression of ACA1-YFP or ACA7-YFP (same transgenes used in [Figure 3](#)) could partially rescue the pollen deficiencies associated with an *aca9* KO mutant, which lacks the most abundant PM-localized ACA in pollen. The *aca9* KO plants have siliques with reduced seed set due to male fertility defects, which is caused by pollen tubes that are short, slow-growing and deficient in their ability to discharge sperm ([Schjøtt et al., 2004](#)). Both ACA1-YFP and ACA7-YFP transgenes were stably expressed in *aca9* ($-/-$) KO plants and displayed expression levels equivalent or better than ACA9-YFP controls, as determined by YFP fluorescence in pollen grains ([Supplemental Figure S2](#)).

Two assays were performed to test whether ACA transgenes could rescue the fertility defects of an *aca9* KO. The first was to test for restoration of normal seed set ([Figure 4A](#)). This bioassay was previously used to corroborate a PM function for ACA12 ([Limonta et al., 2014](#)), and provided a control demonstrating that ER-localized ACA2

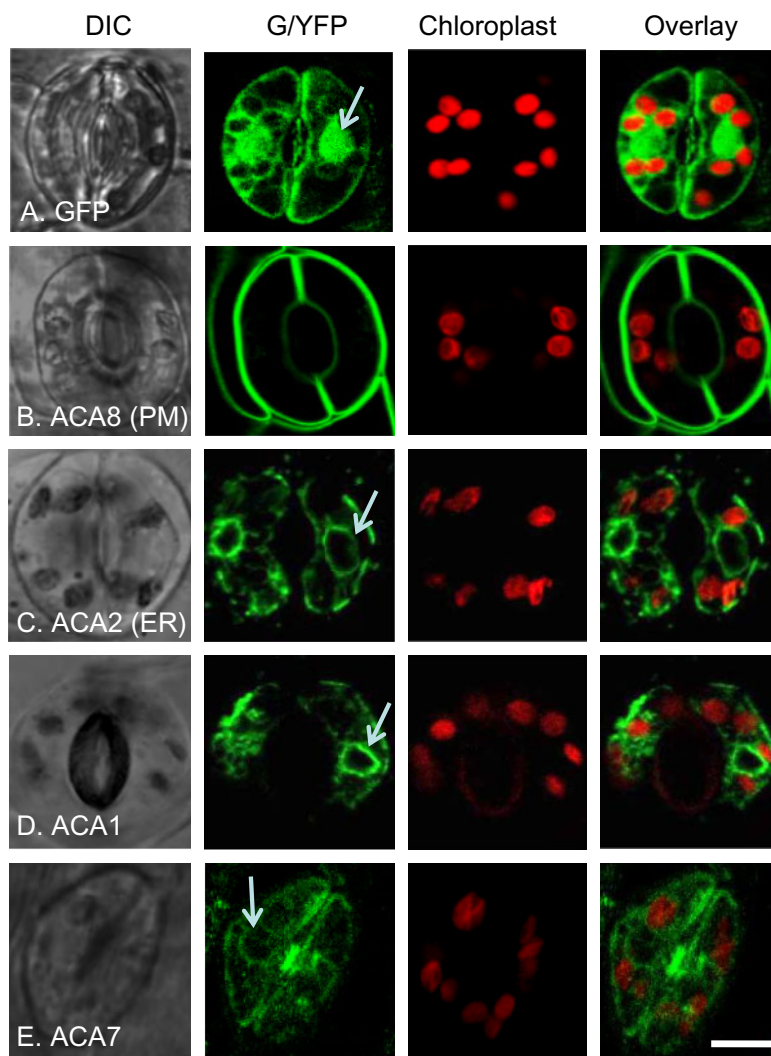


Figure 2 Confocal fluorescence microscopy of guard cells showing FP-tagged ACA1 and 7 with subcellular localizations similar to ER-localized ACA2. The positions of chloroplast were visualized by chlorophyll red autofluorescence and overlaid with GFP or YFP images. White arrows point to ER surrounding the nucleus. A, GFP control showing the pattern of accumulation in the cytosol and nucleus. B, ACA8-GFP showing PM localization. C, ACA2-GFP showing ER localization. D and E, ACA1-YFP and ACA7-YFP showing an endomembrane pattern similar to ACA2-GFP. At least two independent lines were analyzed for each ACA-FP fusion. The expression of all fusion constructs were under the control of a 35S promoter except ACA7-YFP, which was under the control of a *UBQ10* promoter. Corresponding seed stock (ss) numbers and plasmid stocks (ps) are GFP only (ss1811, ps346), ACA8-GFP (ss248, ps396), ACA2-GFP (ss2214–2216, ps660), ACA1-YFP (ss2211–2213, ps1294), and ACA7-YFP (ss2401, ps2628). Scale bar is 10 μ m.

was unable to provide a functional rescue. In agreement with prior results for ACA2, neither ACA1 nor 7 showed any detectable restoration of seed set in the *aca9* KO background (Figure 4A).

As a second approach, a more sensitive genetic segregation analysis was conducted to determine whether hemizygous transgenes could provide a detectable rescue of the *aca9* KO pollen transmission deficiency (Figure 4B). This rescue test was done by comparing the transmission efficiencies of different ACA transgenes through outcrosses or selfing. The segregation of transgenes to F1 progeny was scored by a hygromycin resistance (Hyg^R) marker associated with each transgene. A transmission efficiency ratio (TE_r) was

calculated as the ratio of resistant to sensitive seedlings. In these assays, if a transgene provides a rescue in a mutant *aca9* KO background, then the TE_r would show an increase above that expected for a normal Mendelian segregation. As a control, a transgene encoding PM-localized ACA9 increased TE_r s through a pollen outcross (69-fold) and selfing (2.5-fold), while still showing normal transmission through female gametes (Figure 4B-2). In contrast, we failed to observe any increase in TE_r s (i.e. no rescue) for transgenes encoding ACA1-YFP or ACA7-YFP in selfing (Figure 4B-3), or for ACA7-YFP in pollen outcrosses (Figure 4B-4).

Together, the observed ER localization patterns (Figures 2 and 3) combined with genetic evidence that ACA1, ACA2,

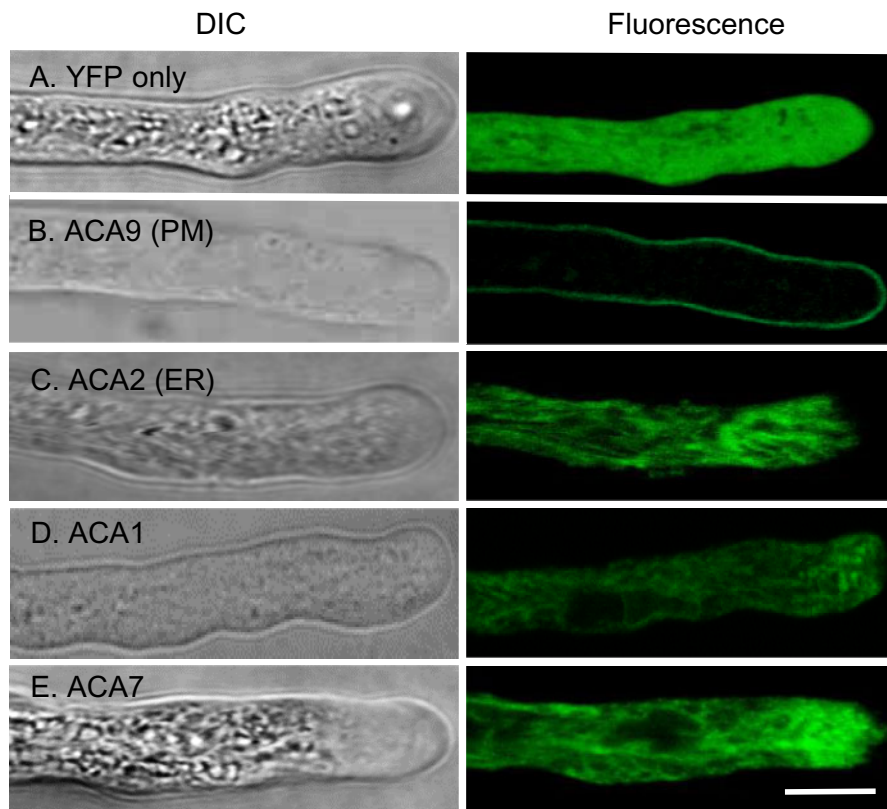


Figure 3 Confocal fluorescence microscopy of pollen tubes showing FP-tagged ACA1 and 7 with subcellular localizations similar to ER-localized ACA2. Pollen tubes were grown in vitro and imaged using confocal microscopy. Bright field (DIC) and fluorescence are shown. A, YFP shows a positive control for cytosolic localization. B, ACA9–YFP shows a control for PM localization (Schjøtt et al., 2004). C, ACA2–GFP shows a comparison for ER localization (Hong et al., 1999). D and E, ACA1–YFP and ACA7–YFP showing an endomembrane pattern similar to ACA2–GFP. At least two independent lines were analyzed for each ACA–FP fusion. The expression of all fusion constructs were under the control of an ACA9 promoter (Schjøtt et al., 2004). Corresponding ss numbers and ps are YFP only (ss2228 and ss2232, ps532), ACA9–YFP (ss2229–2231, ps580), ACA2–GFP (ss2253–2255, ps585), ACA1–YFP (ss2220–2222, ps1295), and ACA7–YFP (ss2249–2252, ps1960). Scale bar is 10 μ m.

and ACA7 are unable to functionally substitute for PM-localized ACA9 (Figure 4) suggest that the ACA1/2/7 subgroup functions primarily at the ER.

Triple KO mutants lacking ACA1, 2, and 7 display impaired pollen fitness

To investigate the biological functions associated with ACA1/2/7, we obtained T-DNA disruption alleles from public collections (Krysan et al., 1996; Sessions et al., 2002; Alonso et al., 2003; Woody et al., 2007; Rosso et al., 2003). Gene models and insertion locations for mutations used here and other studies are shown in Figure 5A and Supplemental Figure S3. Two sets of *aca1/2/7* triple KOs were created by combining independent sets of mutant alleles. The combination of *aca1-2/2-2/7-9* has a mixed parental background comprised of both Columbia-0 (Col-0; *aca2-2*) and Wassilewskija (*WS*; *aca1-2*, *aca7-9*). However, all alleles in the *aca1-7/2-3/7-5* combination were created in a Col-0 parental background. All insertions were in coding-sequence locations predicted to disrupt a functional pump (e.g. missing essential transmembrane domains), except for *aca7-5*. The *aca7-5* insertion occurred in an intron location, which increases the potential for a splicing event to remove

the T-DNA insertion during mRNA processing. However, a qualitative PCR analysis failed to detect transcripts for any of the alleles used in either set of triple mutants (Figure 5B). Thus, both *aca1/2/7* triple mutants have the expectation of being complete loss-of-function KOs.

To test whether single KOs for *aca1*, 2, or 7 by themselves showed any segregation distortion phenotypes, heterozygous plants were subjected to reciprocal outcrosses and selfing (Figure 6, A-1–5). For all individual KOs, reciprocal outcrosses showed no evidence for any transmission deficiencies through either pollen or female gametes. Similarly, there was no distortion observed in selfing of *aca1* or 2. However, *aca7* was a possible exception showing a weak distortion for two different alleles.

In the case of *aca7*, selfing with *aca7-8* and 7-9 alleles revealed that TE_s were slightly lower than expected (2.3 and 2.7, respectively, compared to an expected TE_s of 3, $P < 0.001$; Figure 6, A-4 and 5). However, because reciprocal crosses failed to show any significant transmission deficiency through either male or female gametes (combined across alleles, $n = 1061$, $P = 0.93$ and, $n = 1324$, $P = 0.41$, respectively), the small 0.91- to 0.76-fold decrease in selfing TE_s is most likely related to a zygotic deficiency.

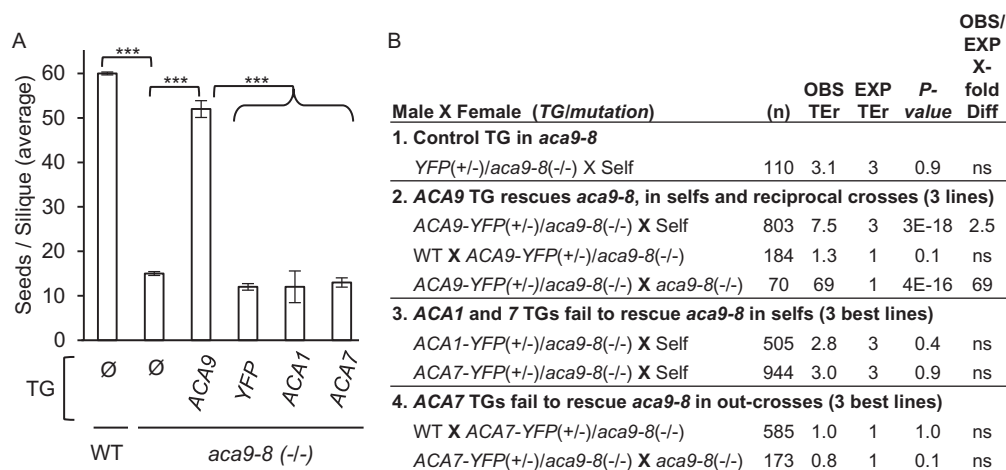


Figure 4 Seed set and genetic segregation analyses showing the inability of transgenes encoding ACA1 and 7 to rescue the KO phenotype for the *aca9* PM Ca²⁺ pump. A, Comparison of the average seed set per silique for selected plants lines expressing a specific transgene (TG) or without (∅). Values represent means ± SD. At least three independent plant lines were quantified with equivalent results for each potential *aca9-8 (-/-)* rescue line expressing TGs encoding ACA9-YFP, YFP, ACA1-YFP, or ACA7-YFP. All plant lines were compared to *aca9-8 (-/-)* mutant. Statistical significance was determined by the Student's *t* test (***) $P < 0.0001$. Not significant denoted as (ns). B, Segregation analyses in an *aca9-8 (-/-)* background and scoring for the transmission of the Hyg^R marker associated with TGs encoding: (1) YFP, (2) ACA9-YFP, (3) ACA1-YFP, and (4) ACA7-YFP. TE_r were calculated by scoring F1 progeny (# Hyg^R over # sensitive) from self-fertilization (Self) or out-crosses. Number of F1 progeny scored denoted by (n). The X-fold difference between observed (OBS) and expected (EXP) TE_rs are shown. Statistical significance was determined by the Pearson's χ^2 with a minimum threshold set at $P < 0.05$. **Supplemental Figure S2** shows the relative TG expression levels in pollen grains as measured by their YFP fluorescence under the microscope. The ACA9 promoter was used to drive the expression of all constructs. Corresponding ss numbers and ps are ACA9-YFP (ss2229–2231, ps580), YFP vector (ss2232–2234, ps532), ACA1-YFP (ss2241–2244, ps1295), and ACA7-YFP (ss2235–2240, ps1960).

Because *aca7* KO mutants were previously reported to show large numbers of aborted pollen grains (Lucca and León, 2012), we further examined the *aca7-1* allele used in that study (Lucca and León, 2012). In our analysis, the same T-DNA source line was backcrossed multiple times and renamed *aca7-10*. Despite using the same T-DNA source line, we failed to detect any transmission decrease in pollen outcrosses, as quantified by PCR genotyping of F1 progeny (TE_r = 1.13 vs an expected of 1, $n = 111$, $P = 0.51$).

In contrast to the weak or non-detectable phenotypes for single KO alleles, the *aca1-2/2-2/7-9* triple KO combination showed a more than two-fold decrease in TE_r, for both selfing ($n = 622$, $P < 9E-22$) and pollen outcrosses ($n = 1296$, $P < 1E-59$), but still showed normal transmission through female gametes (Figure 6A-6). In this assay, the segregation analysis was done by scoring the transmission of a glufosinate herbicide resistance marker (Basta^R) associated with the *aca2-2* allele, which was segregating in a parental background homozygous for *aca1-2* and *aca7-9*.

To confirm that the *aca1/2/7* pollen transmission deficiencies were caused by the combined loss of a redundant ACA activity, hemizygous transgenes encoding ACA1-YFP, ACA2-GFP, and ACA7-YFP (same pollen-specific transgenes used for imaging subcellular localization in Figure 3) were tested for their ability to rescue the male transmission defect of a homozygous *aca1/2/7* triple KO mutant (Figure 6B). This segregation analysis was done by scoring F1 progeny for the transmission of a hygromycin resistance (Hyg^R) marker linked

to the transgenes. In these assays, if a transgene provides a rescue in the *aca1/2/7* KO background, then its TE_r will show an increase above an expected TE_r of 1. In these pollen outcrosses, a TE_r of 2.6 represents an approximate threshold expected for a complete rescue, as estimated from the inverse of the transmission deficiency observed for the segregating *aca2-2* allele (Figure 6A-6). Consistent with evidence for a near or complete rescue, we observed TE_rs ranging from 2.2 to 2.6 for each of the ACA transgenes (Figure 6B), whereas a vector-only transgene showed a normal TE_r.

Triple KO mutants for ACA1, 2, and 7 display SA-dependent rosette size reductions and leaf lesions

Whereas no obvious vegetative growth phenotypes were observed for each of the single KOs, both combinations of *aca1/2/7* triple KOs resulted in smaller rosette sizes, as measured by leaf length (1.2-fold decrease; Figures 7 and 8). These growth reductions were accompanied by an increased frequency of necrotic lesions in leaves (often referred to as a “lesion-mimic phenotype”). To confirm that the observed phenotypes were specifically caused by the *aca1/2/7* mutations, mutant plants were stably transformed with transgenes encoding ACA1-YFP, ACA2-GFP, or ACA7-YFP, with expression under the control of a *Cauliflower mosaic virus-35S* promoter (35S promoter). All of these transgenes were able to reverse the *aca1/2/7* leaf size reductions (Figure 7C). In addition, these transgenes suppressed the increased frequency of leaf lesions, as observed by visual inspection of plants (Figure 7A).

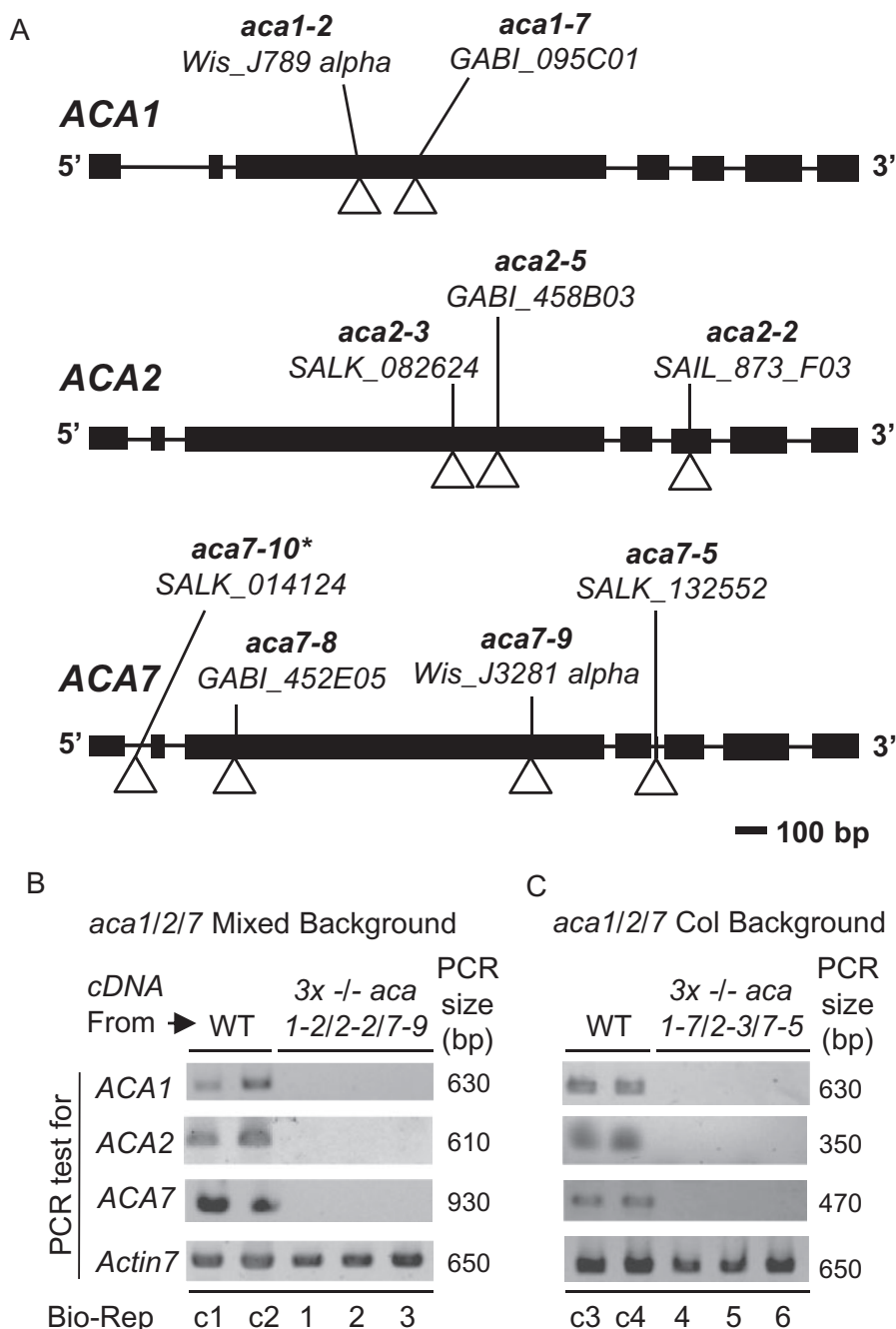


Figure 5 Positions of T-DNA disruptions in gene models for *ACA1*, 2, and 7. A, Gene diagrams for *ACA1* (At2g27770), *ACA2* (At4g37640), and *ACA7* (At2g22950) are shown. The allele name, source, and position of T-DNA insertions are shown. Exons and introns are depicted by boxes and lines, respectively. **aca7-10* is derived from the same source plant as *aca7-1* in (Lucca and León, 2012). B and C, Qualitative PCR showing the presence or absence of detectable mRNA for *ACA1*, 2, and 7 in WT or KO mutants. Two biological replicates (Bio-Reps) are shown for mRNA from WT background controls, WS (control c1 and c2), and Col (c3 and c4). For each KO, 3 biological replicates all show a failure to amplify each *ACA* mRNAs in KO mutants *aca1-2/2-2/7-9* ("Mixed Background") Bio-Reps 1, 2, and 3 (Panel B) and *aca1-7/2-3/7-5* (Col Background) Bio-Reps 4, 5, 6 (Panel C). PCR amplification of *Actin 7* (At5g09810) was used as a normalization control (650 bp fragment generated with primers 2297a + 2297br). For *ACAs*, primers with expected amplicon sizes (PCR size in bp) were *ACA1* (630 bp) primers 2308a + 2308br, *ACA2* (610 bp) primers 2304a + 2304br or (350 bp) primers 2307a + 2306br, *ACA7* (930 bp) primers 875e + 2292 or (470 bp) primers 875g + 2292. The cDNA used was made from equivalent mixtures of mRNA from leaf and pollen tissue. Primer positions and sequences used for genotyping and qualitative PCR analyses are provided in Supplemental Figure S3 and Supplemental Table S2, respectively.

The high frequency of lesions in *aca1/2/7* leaves was accompanied by increases in the expression of transcriptional markers for an SA response (Palmer et al., 2019), including

Pathogenesis-related1 (*PR1*), AT2G14610; Figures 7, D and 8, B) and *PR2* (AT3G57260; Supplemental Figure S4). Additionally, triple KOs showed an increase in the

A.

Male X Female	n	OBS TE _r	EXP TE _r	P-value	OBS/ EXP X-fold Diff
1. <i>aca1-7 (+/-)</i> single KO transmission (Sulf^R)					
<i>aca1-7 (+/-)</i> X Self	263	3.53	3	0.27	ns
WT X <i>aca1-7 (+/-)</i>	1023	0.92	1	0.20	ns
<i>aca1-7 (+/-)</i> X WT	852	0.85	1	0.02	ns
2. <i>aca2-2 (+/-)</i> single KO transmission (Basta^R)					
<i>aca2-2 (+/-)</i> X Self	1160	3.33	3	0.14	ns
WT X <i>aca2-2 (+/-)</i>	242	0.89	1	0.37	ns
<i>aca2-2 (+/-)</i> X WT	1230	1.05	1	0.42	ns
3. <i>aca2-5 (+/-)</i> single KO transmission (Sulf^R)					
<i>aca2-5 (+/-)</i> X Self	696	2.59	3	0.08	ns
WT X <i>aca2-5 (+/-)</i>	252	1.05	1	0.71	ns
<i>aca2-5 (+/-)</i> X WT	160	0.95	1	0.75	ns
4. <i>aca7-8 (+/-)</i> single KO transmission (Sulf^R)					
<i>aca7-8 (+/-)</i> X Self	682	2.29	3	0.001	0.76
WT X <i>aca7-8 (+/-)</i>	592	1.04	1	0.62	ns
<i>aca7-8 (+/-)</i> X WT	855	1.01	1	0.92	ns
5. <i>aca7-9 (+/-)</i> single KO transmission (Kan^R)					
<i>aca7-9 (+/-)</i> X Self	5938	2.72	3	7E-04	0.91
WT X <i>aca7-9 (+/-)</i>	732	0.89	1	0.12	ns
<i>aca7-9 (+/-)</i> X WT	206	1.00	1	1	ns
6. Triple KO <i>aca1-2(-/-)/7-9(-/-)/2-2(+/-)</i> transmission (Basta^R)					
<i>aca1/7(-/-)</i> ; 2-2(+/-) X Self	622	1.40	3	9E-22	0.47
WT X <i>aca1/7(-/-)</i> ; 2-2(+/-)	186	0.88	1	0.38	ns
<i>aca1/7(-/-)</i> ; 2-2(+/-) X WT	1296	0.38	1	1E-59	0.38

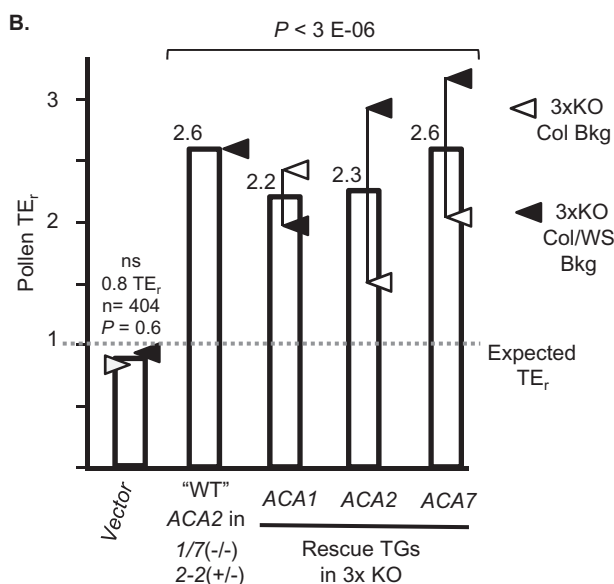


Figure 6 Transmission genetics showing that a triple KO of *aca1/2/7* has a pollen deficiency that can be rescued through pollen-specific expression of transgenes encoding ACA1, 2, or 7. All crosses were conducted using transgenic lines harboring a single hemizygous transgene. All significance testing was done with a Pearson's χ^2 with a minimum threshold set at $P < 0.05$. Not significant denoted as (ns). TE_rs were scored in F1 progeny as # of resistant/# of sensitive seedlings for selection markers associated with T-DNA insertions as indicated (Basta^R, Kan^R, Sulf^R). A, Parts 1–5 show segregation analyses of single KO alleles for *aca1-7* (1), *aca2-2* (2), *aca2-5* (3), *aca7-8* (4), *aca7-9* (5). Part 6 shows segregation analyses for *aca1-2(-/-)/7-9(-/-)/2-2(+/-)* in which the segregation of the hemizygous *aca2-2* allele was scored

expression of diagnostic markers for a pathogen response involving Ca²⁺ signals, including *FRK1* (FLG22-induced receptor-like kinase 1, AT2G19190) and *Phosphate-inducible 1* (PHI1, AT1G35140), consistent with a potential misregulation of Ca²⁺ signals in the triple KO mutant.

To determine if the observed plant growth deficits and lesion phenotypes were due to over-activation of a SA-dependent pathway, as observed in *aca4/11* mutants (Boursiac et al., 2010), we introgressed a transgene encoding NahG (Molina et al., 1998) into the *aca1-2/2-2/7-9* mutant. NahG is an SA-degrading enzyme used by bacterial pathogens to suppress plant defense responses (You et al., 1991; Gaffney et al., 1993; Delaney et al., 1994). NahG expressing lines restored growth and attenuated the lesion phenotype of an *aca1/2/7* KO mutant (Figure 8A). For comparison, phenotypes associated with *aca4/11* KO plants with and without NahG expression are shown in Figure 8, A and B. While the *aca4/11* KO appears to cause a more severe reduction in plant size and lesion frequency, the lesion phenotypes in both *aca4/11* and *aca1/2/7* mutants were equally rescued by the NahG transgene. These results confirm that the lesion-associated growth deficits observed in *aca1/2/7* plants are SA-dependent.

Nutritional supplements can suppress lesion formation in an *aca1/2/7* triple KO

Several nutritional supplements were previously found to suppress the lesion formation in the *aca4/11* KO (Boursiac et al., 2010). To determine whether the same supplements would suppress the lesion phenotype of *aca1/2/7* mutants, young seedlings were grown in a standard hydroponic solution supplemented with 15 mM NH₄NO₃, 15 mM KCl, or 15 mM KH₂PO₄. As previously observed for *aca4/11*, each of the above supplements suppressed any visible lesion formation in *aca1/2/7* mutants and restored rosette growth to that of wild-type controls (Supplemental Figure S5).

by a Basta^R marker. B, Bar graph showing TE_rs associated with pollen transmission of hemizygous rescue constructs. For rescue constructs, TE_rs were calculated based on the transmission of the Hyg^R marker associated with each transgene. For the "WT" ACA2, the TE_r shown represents the endogenous wild-type ACA2 segregating in competition with the *aca2-2* allele, as quantified in part A-6 (inverse of the 0.38 TE_r calculated for *aca2-2*). A dotted line shows the expected TE_r of 1 for normal Mendelian transmission. The average TE_r is shown for the best rescue lines for each of the two triple KO combinations, with open triangles representing rescues in *aca1-7(-/-)/2-3(-/-)/7-5(-/-)* (Col background), and closed triangles representing rescues in *aca1-2(-/-)/2-2(-/-)/7-9(-/-)* (Col/WS mixed background). Corresponding ss numbers and ps are ACA9::YFP (ss2497, ps532 for Col background, ss2224 for Col/WS mixed background), ACA1 (ss2220–2221, ps1295 for Col background, ss2222 for Col/WS mixed background), ACA2 (ss2253 and 2255, ps585 for Col background, ss2498–2500 for Col/WS background), and ACA7 (ss2501, ps1960 for Col background, ss2249–2252 for Col/WS mixed background).

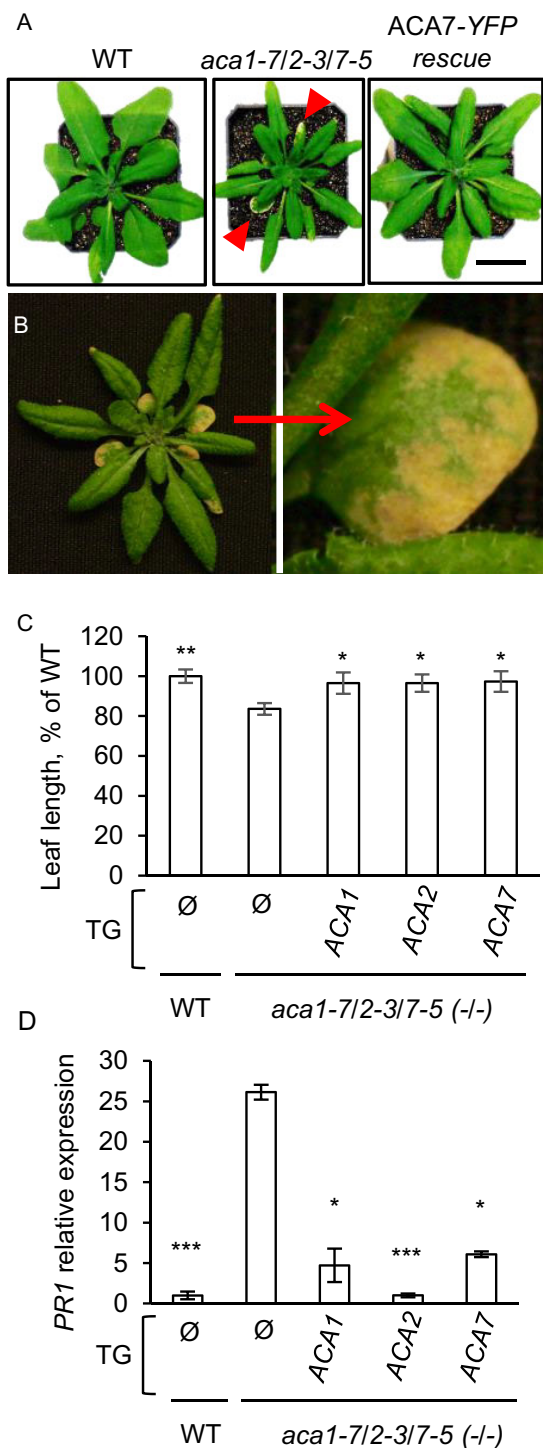


Figure 7 An *aca1/2/7* triple KO results in smaller plants with lesions and increased expression of the *PR1* pathogen response gene. A, Representative rosettes at the time of bolting showing *aca1/2/7* KO plants with smaller leaves, and an *aca1/2/7* mutant rescued by expression of 35S::ACA7-YFP (ACA7-YFP rescue). Red arrows point to lesions. Scale bar is 1 cm. B, An *aca1/2/7* KO plant showing an enlargement of a leaf with lesions. C, Leaf length measurements showing reduced leaf size for an *aca1/2/7* KO compared to WT, and representative examples of mutant plants rescued by transgenes encoding ACA1-YFP, ACA2-GFP, and ACA7-YFP. The three largest rosette leaves were measured at the time of bolting from each plant.

Cotyledons in a triple KO mutant of ACA1, 2, and 7 display altered Ca^{2+} signatures when stimulated by blue light or flg22 peptide

To determine if the loss of ACA1/2/7 could impact cytosolic Ca^{2+} signaling, a transgene encoding a Ca^{2+} sensor (YC-Nano65; Choi et al., 2014) was stably transformed into *aca1-7/2-3/7-5* and a control wild-type background. $[Ca^{2+}]_{cyt}$ transients were triggered in 7-d-old seedlings by exposing cotyledons (pre-adapted to low light) to a continuous blue-light stimulus (Figure 9; Supplemental Movie S2). The initiation of the blue-light exposure resulted in a $[Ca^{2+}]_{cyt}$ transient that peaked within 2 min. In comparison to wild-type, the magnitude and duration of the $[Ca^{2+}]_{cyt}$ transients in *aca1/2/7* cotyledons were increased nearly two-fold to a Fluorescence Resonance Energy Transfer (FRET) ratio around 7.5. Interestingly, mutant lines showed a resting level of $[Ca^{2+}]_{cyt}$ that appeared to be higher at the initiation of the transient and remained higher than wild-type controls for > 90 min after initiating the stimulus (Figure 9C).

YC-Nano65 is a FRET-based reporter that involves an energy transfer from a blue-light excitation of the CFP domain to the neighboring YFP domain (Choi et al., 2014). The magnitude of FRET is increased when Ca^{2+} induces a conformational change that brings the CFP and YFP domains into closer proximity. Two controls were done to ensure that the apparent FRET changes actually represented a Ca^{2+} -dependent event and not an artifact from a direct blue-light excitation of the reporter itself. First, we expressed YC-Nano65 in *Escherichia coli* and exposed bacteria to a blue-light stimulus as done for plants. In contrast to plants, the bacterial YC-Nano65 failed to show any increase in FRET (Supplemental Figure S6), indicating that the YC-Nano65 does not produce an artifact signal under the applied imaging conditions. A second control utilized an alternative $[Ca^{2+}]_{cyt}$ reporter, GCaMP6f (Badura et al., 2014; Supplemental Figure S7). Unlike YC-Nano65, GCaMP6f does not utilize a CFP domain for FRET but instead directly

Values shown are mean \pm SE for measurements from two independent experiments with at least three biological replicates in each experiment. Significance was determined by the Student's *t* test (* $P < 0.05$ and ** < 0.01) in comparison to the un-rescued *aca1/2/7* mutant (TG = ∅). D, RT-qPCR showing expression of a SA-dependent molecular marker gene, *PR1* (AT2G14610). PCR analyses were conducted using 1-week-old seedlings grown on agar plates containing $1/2\times$ MS media plus 0.5% (w/v) sucrose. Seedlings did not show visible lesions at the time of analysis. Mean values are shown \pm SE from two independent experiments with at least three biological replicates in each experiment. *EF1-alpha* (AT5G60390) was used as reference gene for normalization. Significance was determined by the Student's *t* test (* $P \leq 0.05$ and *** ≤ 0.0001) with all genotypes compared to *aca1/2/7*. The triple mutant *aca1-7/2-3/7-5* background was used for (A–D). All fusion constructs were expressed under the control of a 35S promoter. At least two independent lines were analyzed for each rescue with equivalent results. Corresponding ss numbers and ps are ACA2-GFP (ss2214–2216, ps660), ACA1-YFP (ss2211–2213, ps1294), and ACA7-YFP (ss2217 and 2218, ps2091).

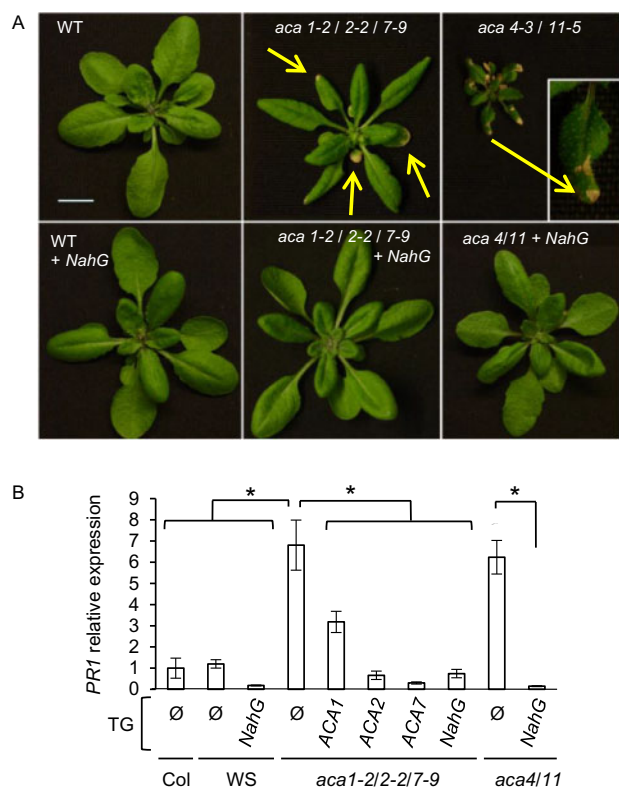


Figure 8 Expression of a SA degrading enzyme, NahG, attenuates lesion phenotypes in *aca* KO plants. A, Pictures of rosettes at time of bolting showing an *aca1/2/7* triple KO plant in parallel with wild type (WT) and *aca4-3/11-5* KO mutant with and without expression of a *NahG* transgene. Plants were grown in parallel under same greenhouse conditions. Yellow arrows mark examples of lesions. Inset shows a magnified leaf with lesions. Scale bar is 1 cm. B, RT-qPCR showing *PR1* transcript abundance. Mean values are shown \pm SE from three independent experiments with three biological replicates in each experiment. Student's *t* test was performed to compare the relative expression of *PR1* in WT and rescue lines of *aca1-2/2-2/7-9* and *aca4-3/11-5* mutants, $P < 0.05$ (*). The *NahG* transgene is in wild-type WS parental background while *ACA1/2/7* rescue lines are in a mixed background resulting from combining insertions identified in WS and Col-0 parental backgrounds. All fusion constructs were expressed under the control of a 35S promoter. At least two independent lines were analyzed for each *ACA* transgene with equivalent results. Corresponding ss numbers and ps are *aca4-3/11-5* (ss316), WT + *NahG* (ss506), *aca4-3/11-5* + *NahG* (ss811), *aca1-2/2-2/7-9* + *NahG* (ss2144), *ACA2-GFP* (ss2214–2216, ps660), *ACA1-YFP* (ss2211–2213, ps1294), and *ACA7-YFP* (ss2502–2503, ps2091).

couple a change in GFP fluorescence to a Ca^{2+} -dependent conformational change in a calmodulin domain. Consistent with the YC-Nano65 reporter, the GCaMP6f reporter confirmed a similar blue-light triggered Ca^{2+} transient in wild-type cotyledons.

Additional controls provided evidence that the *aca1/2/7*-dependent amplification of blue-light Ca^{2+} responses was not a secondary artifact related to increases in SA signaling. Because SA has been implicated in multiple stress responses (Klessig et al., 2018), there is a possibility that *aca1/2/7*-triggered changes in SA signaling might indirectly impact some

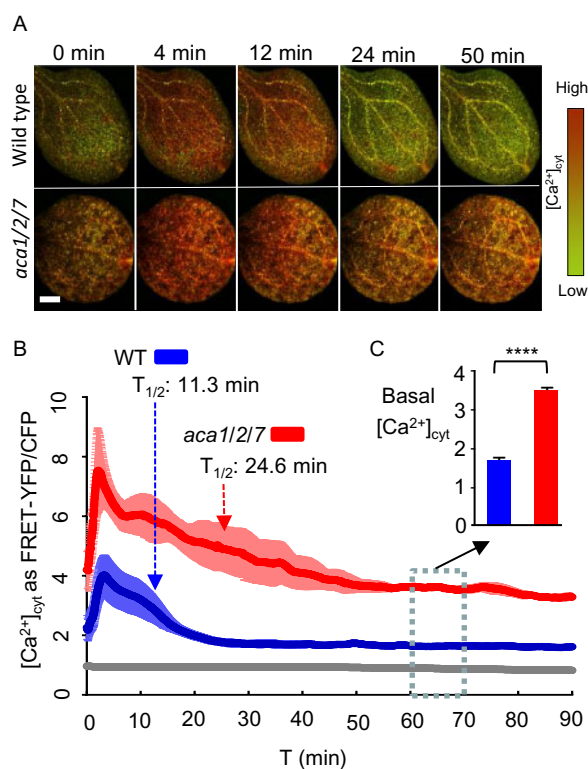


Figure 9 FRET imaging of YC-Nano65 showing that WT and *aca1/2/7* seedlings differ in the Ca^{2+} dynamics triggered by blue-light stimulus. Blue-light-triggered $[\text{Ca}^{2+}]_{\text{cyt}}$ changes were monitored using a YC-Nano65 reporter stably expressed in WT and an *aca1/2/7* mutant. Analyses shown were conducted using 7-d-old cotyledons. Plants were allowed to adapt to dim light for at least 1 h prior to initiating a continuous blue-light stimulus at time zero (ex440/40 nm with $24 \mu\text{mol m}^{-2}\text{s}^{-1}$ intensity). Images were captured every 2 s for 90 min. A, Representative images showing a time series of FRET-YFP/CFP ratios in leaves from WT and *aca1/2/7*. Scale bar is 0.5 mm. B, Graph showing quantitative measurements of blue-light-triggered $[\text{Ca}^{2+}]_{\text{cyt}}$ transients in leaves from WT (blue) and *aca1/2/7* (red). The gray line represents the changes observed with a WT plant without any YC-Nano65. Ratiometric data from FRET-YFP/CFP signals were extracted from the entire leaf surface. Error bars (shading around lines) represent SEM of $n = 5$ plants (WT) or 4 plants (*aca1/2/7*). $T_{1/2}$ arrows mark the time required to restore $[\text{Ca}^{2+}]_{\text{cyt}}$ to half the peak intensity. C, Average basal $[\text{Ca}^{2+}]_{\text{cyt}}$ levels are shown from 60 to 70 min, with error bars showing SEM from total of $n = 1,500$ measurements for WT or 1200 measurements for *aca1/2/7* plants based on five (WT) or four (*aca1/2/7*) independent seedlings. Statistical analyses were done using Student's *t* test. **** indicates $P < 0.0001$. Equivalent results were seen for two independently generated YC-Nano65 reporter lines for both the *aca1/2/7* mutant and WT control. Corresponding ss numbers for plants expressing the transgene 35S::YC-Nano65 (ps2151) are ss2444–2445 for WT Col, and ss2446–2447 for *aca1-7/2-3/7-5*.

stimulus-specific Ca^{2+} responses. To evaluate this potential, we compared the Ca^{2+} transients in KO plants with and without a transgene encoding NahG, an SA-degrading enzyme (You et al., 1991; Gaffney et al., 1993; Delaney et al., 1994). This same *NahG* transgene attenuated the SA-dependent lesion formation shown in Figure 8. Regardless of the presence or absence of *NahG*, FRET imaging showed a

similar amplification of blue-light triggered Ca^{2+} transients as well as a baseline $[\text{Ca}^{2+}]_{\text{cyt}}$ that was about two-fold higher than wild-type (Supplemental Figure S8). While this result does not rule out the potential for SA-dependent modifications of Ca^{2+} signals in the context of other tissues or stimuli, it provides strong evidence that the *aca1/2/7*-dependent amplification of a blue-light triggered Ca^{2+} response in cotyledons is a direct consequence of disruptions in the ER-localized Ca^{2+} pumps and not an indirect effect of SA.

To determine if the *aca1/2/7* KO amplified other types of stimulus-dependent Ca^{2+} signals, young seedlings were tested for changes in their response to flg22, a peptide corresponding to a conserved domain in bacterial flagellins that is known to elicit pathogen responses (Sun et al., 2006; Miché et al., 2018; Tena, 2019). To facilitate the rapid infusion of flg22 into leaves, a wound site was created the day before elicitor application. Before adding flg22, plants were pre-adapted for at least 1 h to the blue-light excitation conditions required for FRET imaging with YC-Nano65, allowing the $[\text{Ca}^{2+}]_{\text{cyt}}$ to return to a baseline after initial blue-light stimulation. This pre-adaptation was needed to separate an initial blue-light triggered response from a secondary elicitor response. In a comparison to a mock control, flg22 triggered a Ca^{2+} transient that rose two-fold above basal levels to a peak (FRET ratio ~ 4) after about 10 min (Figure 10; Supplemental Figure S9). In contrast, the magnitude of the elicitor triggered $[\text{Ca}^{2+}]_{\text{cyt}}$ transients in *aca1/2/7* leaves increased more than two-fold to a FRET ratio of 10 (Figure 10), which was more dramatic than the blue-light triggered responses shown in Figure 9 (peak FRET ratio ~ 7.5). Similar to the imaging of blue-light Ca^{2+} responses, the mutant showed a resting level of $[\text{Ca}^{2+}]_{\text{cyt}}$ that appeared to be higher at both the initiation and completion of the Ca^{2+} influx/efflux cycle (Figure 10C), suggesting a persistent increase in the average resting levels of $[\text{Ca}^{2+}]_{\text{cyt}}$. Thus, two independent sets of stimuli demonstrate the importance of the ACA1/2/7 subgroup of ER-localized Ca^{2+} pumps in the attenuation of $[\text{Ca}^{2+}]_{\text{cyt}}$ transients.

Discussion

The Arabidopsis genome encodes 10 ACA-type Ca^{2+} pumps that cluster into four phylogenetically conserved groups (P2B-1, -2, -3, -4; Baxter et al., 2003; Pedersen et al., 2012). Genetic and subcellular localization results here provide evidence that members of the P2B-1 subgroup, ACA1, 2, and 7, are all functionally interchangeable and reside primarily in the ER. This information expands an analysis of representative ACAs to support a classification in which members of the P2B-1 subgroup (e.g. ACA1/2/7) share a primary subcellular location corresponding to the ER, whereas the P2B-2 subgroup (e.g. ACA4/11) localize to the vacuole, and the P2B-3 and P2B-4 groups reside primarily at the PM (see Figure 1).

While KO phenotypes have now been documented for different subgroups of ACAs, it is important to note that

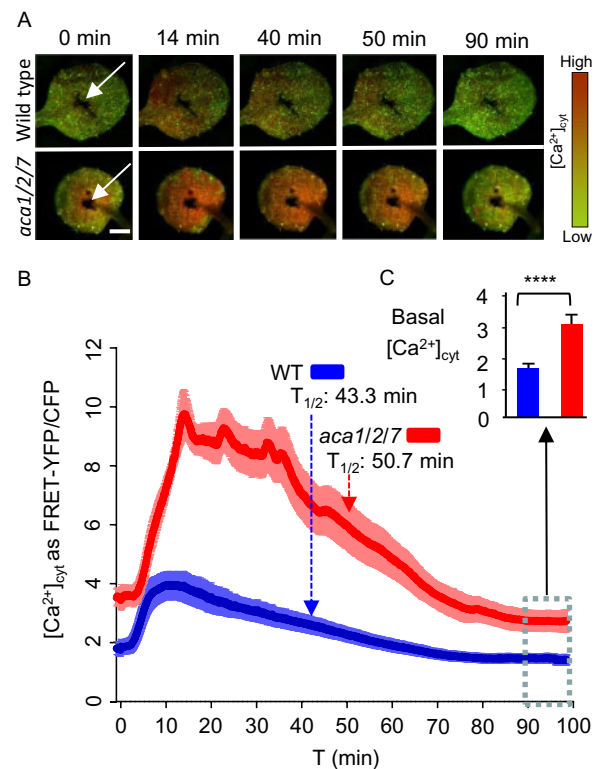


Figure 10 FRET imaging of YC-Nano65 showing WT and *aca1/2/7* seedlings differ in Ca^{2+} dynamics triggered by a pathogen elicitor. Flg22 pathogen elicitor-triggered $[\text{Ca}^{2+}]_{\text{cyt}}$ changes were monitored using a YC-Nano65 reporter stably expressed in WT and an *aca1/2/7* mutant. Analyses shown were conducted using the first true leaves from 2-week-old seedlings. On the day before imaging, a wound site (white arrows, Panel A) was created with a tweezer tip. The wound site was created to permit the direct infiltration of an elicitor solution into surrounding cells. Immediately prior to imaging, seedlings were allowed to adapt to a continuous blue-light exposure (ex440/40 nm with $24 \mu\text{mol m}^{-2}\text{s}^{-1}$ intensity) for at least 1 h. After application of 500 nM flg22 elicitor (in 2 μL), images were captured every 2 s for 100 min. A, Representative images showing a time series of FRET-YFP/CFP ratios in leaves from WT and *aca1/2/7* after exposure to flg22. Indicated time (min) correspond to points graphed in panel “B” to show the time course of $[\text{Ca}^{2+}]_{\text{cyt}}$ changes. Scale bar is 0.5 mm. B, Graph showing quantitative ratio of $[\text{Ca}^{2+}]_{\text{cyt}}$ changes for WT (blue) and *aca1/2/7* (red) in response to flg22 applied at time zero. Ratiometric data from the FRET-YFP/CFP signals were extracted from the entire leaf surface. Error bars are SEM from $n = 8$ independent seedlings. Dashed lines with arrows mark the half time of $[\text{Ca}^{2+}]_{\text{cyt}}$ decay from the peak to basal levels. C, Average basal $[\text{Ca}^{2+}]_{\text{cyt}}$ levels after a recovery from a flg22 elicitor-triggered $[\text{Ca}^{2+}]_{\text{cyt}}$ signature. The basal levels were calculated by averaging ratio data from the 90–100 min time period (blue dashed line box, total 300 time points each) in “B”. Error bars are SEM from $n = 2400$ measurements each for *aca1/2/7* or WT based on an analysis on eight independent seedlings. Statistical analysis was done using Student’s t test. **** indicates $P < 0.0001$. Plant lines used and corresponding ss numbers are the same as identified in Figure 9.

there are different potential mechanistic explanations: The first is through pump deficiencies changing the local efflux dynamics of Ca^{2+} transients, and the second by changing

the steady-state levels of $[Ca^{2+}]$ in a specific compartment (i.e. a Ca^{2+} nutrition function; Spalding and Harper, 2011). Results here support an important role for ER ACAs in shaping the dynamics of multiple Ca^{2+} signals but do not rule out a potential role in Ca^{2+} homeostasis in the ER or secretory pathway (Himschoot et al., 2017).

ACA1, 2, and 7 show ER-like subcellular locations

Four lines of evidence support the contention that ACA1, 2, and 7 share an ER-like subcellular localization. First, an ER location for ACA2 was previously established based on immunocytochemistry, subcellular fractionation, and corroboration through confocal imaging of an ACA2–GFP fusion in root cells (Hong et al., 1999). Second, ACA1 and 2 were both shown in a proteomics analysis to be enriched in an ER subcellular fraction in which proteins were identified and quantified by mass spectrometry (Dunkley et al., 2006). ACA7 was not detected in this proteome analysis, most likely because of its low abundance in the vegetative tissues used for cellular fractionation. Third, confocal microscopy here corroborates that each FP-tagged ACA shows a similar ER-like localization in both vegetative cells and pollen (Figures 2 and 3). Lastly, the ability of each ACA to rescue phenotypes associated with the *aca1/2/7* triple KO in both pollen and vegetative cells (Figures 6–8) provides strong evidence that each isoform has the ability to accumulate and interchangeably function in an ER-location similar to ACA2.

The assignment of an ER location for ACA1 and 7 differs from previously suggested locations for ACA1 in the chloroplast (Huang et al., 1993) and ACA7 in the PM (Lucca and León, 2012). In the case of ACA1, a previous assignment was determined by probing cell fractions with a polyclonal antibody that might have recognized multiple P-type ATPase proteins (Huang et al., 1993). Nevertheless, to address a chloroplast targeting potential, we examined the localization of ACA1–YFP in guard cells where chloroplast autofluorescence can be used as a co-visualization marker. In difference to (Huang et al., 1993), we failed to find any evidence for colocalization of ACA1–YFP with chloroplasts (Figure 2). Instead, a different P-type ATPase, HMA1, has since been shown to target to the chloroplast envelope and appears to function as both a heavy metal and Ca^{2+} pump (Seigneurin-Berny et al., 2006; Moreno et al., 2008; Kim et al., 2009).

In the case of ACA7, a previous PM-localization assignment was based on confocal imaging of a GFP–ACA7 fusion transiently over-expressed using a 35S promoter in *N. benthamiana* leaf epidermal cells (Lucca and León, 2012). This transient expression study differed from experiments here in several important ways: (1) The ACA7 FP-tags were located at opposite ends of the protein, with an N-terminal location used by (Lucca and León, 2012) and a C-terminal location used here. While it is not clear if a difference in tag location might alter targeting, the N-terminal end of ACA7 harbors a regulatory autoinhibitory domain that could be compromised by fusion to a FP-tag. (2) The ACA7–YFP used here was stably transformed into plants and functionally rescued *aca1/2/7* KO phenotypes (Figures 6–8) to the

same extent as an established ER-localized ACA2. In contrast, the transient expression analyses done by (Lucca and León, 2012) were not corroborated with any functional assays. (3) To test for a potential secondary PM function for ACA7, we also examined whether an ACA7–YFP transgene could rescue a KO of an established PM-targeted ACA9 pump. However, we failed to obtain any evidence for even a partial rescue (Figure 4). It is noteworthy that the retargeting of a PM ACA8 to the vacuole functionally rescued a vacuolar *aca4/11* KO, providing an expectation that different ACAs are interchangeable in different subcellular locations (Hilleary et al., 2020). Given the artifact potentials that might arise from using transient over-expression of fusion proteins (Moore and Murphy, 2009), we favor evidence here that supports an ER localization based on stable expression of fusion proteins that were all able to functionally rescue a triple *aca1/2/7* KO. Nevertheless, it is possible that any given ACA pump might still function in additional locations or show alternative targeting under different environmental or experimental conditions.

ACA1/2/7 are important for pollen fitness

Results here revealed that a triple *aca1/2/7* KO displays a pollen transmission deficiency (Figure 6). In a genetic segregation analysis, the pollen transmission of an *aca1/2/7* triple KO showed a 2.6-fold decrease in transmission efficiency (Figure 6). This deficiency appeared to be specific to pollen, as normal Mendelian segregation was observed through female gametes. While it is not yet clear which aspects of pollen development or fertilization specifically require these pumps, pollen tubes are one of the most rapidly growing cells (Stone et al., 2004), with a high demand on ER/secretory systems and a dependence upon multiple Ca^{2+} signaling systems to coordinate growth processes that allow a pollen grain to germinate on the stigma and undergo tip growth to reach an ovule and discharge sperm cells (Obermeyer and Feijó, 2017; Johnson et al., 2019). As an indication of the complexity of this journey, there are at least 39 putative Ca^{2+} permeable channels expressed in pollen that could lead to Ca^{2+} transients that require the efflux activities of Ca^{2+} pumps and CAXs at multiple subcellular locations (Johnson et al., 2019).

In the context of single KO phenotypes, we failed to find any evidence to support a pollen lethality phenotype previously predicted from an analysis of *aca7-1* and *7-2* alleles by (Lucca and León, 2012). In this previous study, Alexander staining detected a pollen abortion frequency as high as 65% in anthers from *aca7-1* or *aca7-2* homozygous mutants, in contrast to a near 0% abortion for wild-type controls. If this pollen lethality were due to a pollen autonomous defect, the expectation is that it should result in a severe TE_r deficiency in pollen outcrosses. However, we failed to see any pollen transmission distortion for the two null-alleles assayed here, *aca7-8* and *aca7-9*, as well as the *aca7-1* allele analyzed by (Lucca and León, 2012; combined $n = 1172$, $P = 0.93$, Figure 6A-4 and 5 and *aca7-1* results in text). Nevertheless, an analysis of selfing for *aca7-8* and *aca7-9*

revealed a small 1.1- and 1.3-fold decrease in TE_s, respectively ($P < 0.001$; Figure 6A-6). However, because the reciprocal crosses failed to show any transmission deficiencies through male or female gametes, this small selfing distortion most likely represents a zygotic defect, supporting a potential for additional ACA7-related phenotypes in cell types other than pollen.

ACA1, 2, and 7 are important for vegetative development

In addition to a pollen reproductive phenotype, the triple KO resulted in smaller plants displaying leaves with an increased frequency of lesions, as well as a molecular phenotype characterized by the induction of *PR1* and *PR2* mRNAs, which are transcriptional markers for an SA signaling response (Figures 7 and 8; Supplemental Figure S4). Both smaller leaves and lesion phenotypes were suppressed by the introduction of a *NahG* transgene (Figure 8), which encodes an enzyme that degrades SA into the relatively inert catechol (You et al., 1991; Gaffney et al., 1993; Delaney et al., 1994). This suggests that a reduction in the capacity for ER Ca²⁺ pump activity somehow potentiates the production of SA, which can inhibit plant growth and trigger programmed cell death.

A similar lesion phenotype was also reported for a double KO of two vacuolar Ca²⁺ pumps, ACA4 and 11 (Boursiac et al., 2010). While *aca4/11* lesions appear more severe than *aca1/2/7*, growth defects in both mutant sets were fully rescued by the addition of a *NahG* transgene (Figure 8), suggesting both mutants display growth reductions dependent on elevations in SA signaling. Lesion phenotypes associated with both *aca4/11* (Boursiac et al., 2010) and *aca1/2/7* mutants (Supplemental Figure S5) appear to be fully rescued under hydroponic growth conditions that increase the concentrations for a subset of inorganic nutrients (NH₄NO₃, KCl, or KH₂PO₄). While the mechanism of this nutrient suppression is not clear, it suggests an important feedback interaction between ion homeostasis mechanisms and Ca²⁺ signaling systems.

Another similar lesion phenotype was reported for *N. benthamiana* lines that silenced *NbCA1* using RNAi (Zhu et al., 2010). While an ER localization was proposed for *NbCA1* based on transient expression of an *NbCA1*-citric-tagged fusion, the overall protein sequence identity of *NbCA1* is more closely related to the vacuole-localized AtACA4 and 11, raising a question of whether the lesion phenotype resulted from specifically silencing an ER or vacuolar pump or a combination of multiple pumps. Regardless, it appears that disrupting the ACA Ca²⁺-efflux machinery at either the vacuole or ER potentiates cellular perturbations that can trigger an SA-dependent cell death pathway.

ACA1, 2, and 7 are interchangeable in rescuing vegetative and pollen transmission phenotypes

The creation of an *aca1/2/7* triple KO provided an opportunity to genetically demonstrate that ACA1, 2, and 7 all have

interchangeable activities that can rescue both vegetative and reproductive phenotypes (Figures 6–8). In contrast, members of this subgroup were unable to suppress phenotypes associated with the loss of the PM-localized ACA9. This indicates that ACA1, 2, and 7 (from the P2B-1 subgroup) all share biochemical activities with high levels of redundancy. Nevertheless, this does not exclude the possibility that one or more of these ACAs has unique features important to specific cellular processes not evaluated in this study.

ACA1, 2, and 7 are important for regulating the magnitude and duration of a Ca²⁺ transient

Ca²⁺ imaging indicated that a triple *aca1/2/7* KO can increase the magnitude and duration of [Ca²⁺]_{cyt} transients in leaf cells, as shown with two stimulus-specific triggers, blue light (Figure 9) and a *flg22* pathogen elicitor (Figure 10). These analyses were done using a stably expressed genetically encoded Ca²⁺ sensor, YC-Nano65. In responses to both blue light and *flg22* elicitor, the magnitude and duration of the [Ca²⁺]_{cyt} transients in the triple KO were amplified by as much as two- to three-fold. As such, this study establishes the importance of the ER-localized ACA1/2/7 subgroup in shaping the dynamics of Ca²⁺ signals in plants.

Recently, a similar phenomenon was reported for mutants deficient in the vacuole-localized ACA4 and 11, which showed similar increases in the magnitude and duration of [Ca²⁺]_{cyt} transients in response to *flg22* (Hilleary et al., 2020). Additionally, the RNAi silencing experiment targeting the *N. benthamiana* Ca²⁺ pump *NbCA1*, which is most similar to ACA4 and 11, was also reported to amplify [Ca²⁺]_{cyt} transients triggered by a cryptogein elicitor (Zhu et al., 2010). Thus, both ER and vacuolar ACAs appear to contribute to Ca²⁺ signaling dynamics related to a pathogen elicitor response.

While results here demonstrate that an *aca1/2/7* KO can cause a more than two-fold increase in the magnitude of a *flg22*-triggered [Ca²⁺]_{cyt} transient, it was not initially apparent that such a large change would be observed. The reason is that plant cells have multiple Ca²⁺ efflux systems, including ECAs, CAXs, and other ACAs in different membrane locations, including the vacuole and PM (Demidchik et al., 2018; Kudla et al., 2018). In addition, ACAs that traffic to the PM and vacuole are initially inserted into the ER. Thus, the ability to visualize a [Ca²⁺]_{cyt} change suggests that the resident ACA1/2/7 pumps either account for a large fraction of the total Ca²⁺ efflux capacity in the cell or that each of the multiple efflux pathways is at least partially limited to controlling different micro-environments of [Ca²⁺]_{cyt} (Lopreiato et al., 2014). For example, it is possible that Ca²⁺ released around the ER is slow to diffuse to other parts of the cell and is therefore highly dependent on local efflux systems to restore [Ca²⁺]_{cyt} to lower resting levels in this specific micro-environment. In this scenario, a local rise in [Ca²⁺]_{cyt} might be sufficiently insulated from alternative

efflux pathways to allow a sustained local activation of a YC-Nano65 Ca^{2+} reporter. While questions related to micro-environments await further investigation, the *aca1/2/7*-dependent increases in $[\text{Ca}^{2+}]_{\text{cyt}}$ clearly support an important role for ER-localized ACAs in regulating cellular Ca^{2+} dynamics in plants.

A potential mechanism for *aca1/2/7*-dependent lesion formation

It is not yet clear why a loss of *aca1/2/7* ER pumps, or the *aca4/11* vacuolar pumps, result in an increased frequency of SA-dependent lesions in leaves. However, evidence here indicates that a reduction in ER Ca^{2+} -pump efflux capacity can result in stimulus-specific $[\text{Ca}^{2+}]_{\text{cyt}}$ transients with greater magnitudes and durations (Figures 9 and 10). Similar over-amplification of a flg22-triggered Ca^{2+} signal was reported for a double KO of the vacuolar pumps *aca4/11* (Hilleary et al., 2020). A simple speculation is that a chronic over-amplification of Ca^{2+} transients in response to normal developmental and environmental signals (such as changes in light) eventually trigger cells to respond as if they are under stress.

Consistent with this chronic-stress-signaling hypothesis, *aca1/2/7* seedlings showed elevated expression for two marker genes, *FRK1* and *PHI1*, which represent diagnostic markers for a Ca^{2+} -dependent pathogen defense response (Boudsocq et al., 2010; Supplemental Figure S4). However, a study on a vacuolar *aca4/11* mutant failed to observe a similar induction of these markers, suggesting that a specific activation of this pathway might not be obligatory to lesion development (Hilleary et al., 2020). Nevertheless, a mis-regulation of Ca^{2+} signals might alter transcription factors that are proposed to be inhibited or activated by Ca^{2+} /calmodulin, such as Calmodulin-binding Transcription Activators or Calmodulin-binding protein60s (Du et al., 2009; Wang et al., 2009; Poovaiah et al., 2013; Truman et al., 2013; Seyferth and Tsuda, 2014). These transcription factors are involved in regulating transcription of genes involved in SA biosynthesis. While a question has been raised as to whether Ca^{2+} signals actually change the activities of these transcription factors (Fromm and Finkler, 2015), the chronic mis-regulation of Ca^{2+} signals is likely to disrupt many cellular processes, some of which could mimic stress-signals that normally trigger SA biosynthesis. The over-production of SA can then induce programmed cell death, which results in a lesion-phenotype similar to what occurs in some pathogen defense responses (i.e. hypersensitive response; Bruggeman et al., 2015; Radojčić et al., 2018).

Role of ACA1, 2, and 7 in a blue-light response

Blue-light signals are important for plant development and responses to the environment. There are at least three types of blue-light receptors in flowering plants: phototropins (PHOTs), cryptochromes (CRYs), and the zeitung (ZTL) family of E3-Ubiquitin ligases (Sanchez et al., 2020). Of these, only PHOTs have been shown to trigger a cytosolic Ca^{2+} transient (Harada and Shimazaki, 2007). Importantly, PHOT-

dependent Ca^{2+} signals are followed by an extended period of desensitization (refractory period >2 h; Iino, 1988; Janoudi and Poff, 1991, 1993; Baum et al., 1999). Arabidopsis contains two PHOTs that together mediate responses to both low and high-fluence blue light. While PHOTs likely have multiple functions in different cellular locations, pharmacological evidence suggests that the dominant Ca^{2+} release event occurs through a Ca^{2+} -induced Ca^{2+} -release (CICR) mechanism (Harada and Shimazaki, 2007). This CICR process involves an initial activation of PM-localized Ca^{2+} channels by PHOT1 and 2, but also a PHOT2-specific triggering of phospholipase C (PLC)-derived signals (e.g. diacylglycerol and/or inositol 1, 4, 5-trisphosphate (IP_3)), that are then relayed to other organelles (e.g. vacuole, ER) to further induce intracellular Ca^{2+} release.

Evidence here is consistent with a role of PHOTs in triggering the observed blue-light Ca^{2+} signals. The blue-light intensity used to image the YC-Nano65 reporter ($24 \mu\text{mol m}^{-2}\text{s}^{-1}$) falls within the midrange of PHOT stimulation (0.1 – $250 \mu\text{mol m}^{-2}\text{s}^{-1}$; Harada et al., 2003; Harada and Shimazaki, 2007; Zhao et al., 2013). We also observed a single Ca^{2+} transient followed by a desensitization period lasting for more than 3 h (Figure 9), similar to the refractory periods associated with PHOT signaling (Harada and Shimazaki, 2007). However, this refractory period did not prevent a separate stimulus-specific signal being triggered by the addition of flg22 (Figure 10). This indicates that the refractory period observed in our experiments was specific to the blue light-stimulated Ca^{2+} signals, and not a general interruption of all Ca^{2+} -signaling circuits. While PHOTs are the primary mechanism behind rapid blue-light responses, the absence of PHOTs does not fully eliminate the blue-light Ca^{2+} signals in Arabidopsis (Harada et al., 2003), suggesting other blue light-sensitive receptors contribute at least partially to these pathways.

Regardless of which blue-light receptors are responsible for the stimulation of Ca^{2+} signals in this study, the observation that a deficiency in ER-localized Ca^{2+} pumps (*aca1/2/7*) amplifies blue-light-stimulated Ca^{2+} signals supports a model in which the proposed CICR pathway involves the ER, either as the source of Ca^{2+} or location of Ca^{2+} pump activity that shapes the information content of the signal. It is not yet clear if a disruption of the vacuolar *aca4/11* pumps has a similar impact on blue-light signaling.

Efflux—the ending shapes the message

While both Ca^{2+} influx and efflux pathways are required to create Ca^{2+} signals, determining the extent to which ACA activities impact different Ca^{2+} -dependent processes is a challenge. In the case of ER-localized ACAs from the P2B-1 subgroup, evidence here indicates that a complete KO reduces the Ca^{2+} -efflux capacity and results in an over-amplification of blue-light and flg22-triggered Ca^{2+} signals. However, the biological consequences of over-amplifying these specific signals remain to be elucidated. It is possible that a two- to three-fold signal amplification will not always change the information encoded by a Ca^{2+} transient. By

analogy, a human voice can deliver the same message with a loud yell or a quiet whisper. Nevertheless, KO of either the ER or vacuolar pumps show an SA-dependent lesion phenotype, providing strong support that at least some Ca^{2+} -dependent signaling processes in plants require modulation by ACAs.

Whether more subtle changes in ACA activities will alter Ca^{2+} -signaling have yet to be established. However, it is noteworthy that most ACAs contain an N-terminal autoinhibitory domain that enables these pumps to be turned on or off. The exceptions are ACAs from the P2B-3 subgroup, which appear to have a truncated N-terminal domain (Boursiac and Harper, 2007). A speculation is that these exceptions are regulated at the level of transcription or protein stability or have evolved alternative regulatory mechanisms. For the ACAs with intact autoinhibitors, there is a growing list of potential mechanisms for regulating their activities, including activation by Ca^{2+} /calmodulin (Malmström et al., 1997; Harper et al., 1998) or calmodulin-like proteins (Astegno et al., 2017), activation or inhibition by Ca^{2+} -dependent protein kinases (Hwang et al., 2000; Giacometti et al., 2012; Costa et al., 2017), or activation by other regulatory proteins, such as BONs 1, 2 and 3 (Yang et al., 2017; Li et al., 2018), members of the copine family characterized by two Ca^{2+} -dependent phospholipid-binding C2 domains (Wang et al., 2020). Interestingly, all of these regulatory components are associated with pathways linked to Ca^{2+} , highlighting ACAs a primary target of regulation by the very Ca^{2+} signals they help to create. These potential feedback mechanisms emphasize the importance of ACAs as dynamic partners alongside Ca^{2+} channels in shaping the magnitude and duration of Ca^{2+} signals in plants.

Materials and methods

Plant growth conditions

Arabidopsis (*Arabidopsis thaliana*) seeds were surface sterilized for 3 h with chlorine gas (Clough and Bent, 1998) and germinated on $\frac{1}{2}\times$ Murashige and Skoog (MS) medium containing 0.5% (w/v) sucrose, 0.05% (w/v) 4-morpholineethanesulfonic acid (MES), and 1% (w/v) agar. After 48 h vernalization at 4°C, the seeds were exposed to 130–150 $\mu\text{mol m}^{-2} \text{s}^{-1}$ constant light at room temperature (22°C–23°C). After 10 d, the resulting seedlings were transferred to soil (Sunshine SMB-238; SunGro Horticulture), supplemented with pesticide (Marathon; OHP) and a Turf and Ornamental Systemic Fungicide (Cleary). The plants were grown in growth chambers with temperature and light intensity of 22°C and 130–150 $\mu\text{mol m}^{-2} \text{s}^{-1}$, respectively, for 16-h light and 8-h dark period.

For growing plants under hydroponic conditions, 9-d-old seedlings grown on $\frac{1}{2}\times$ Murashige and Skoog (MS) agar plates were transferred to a foam raft in magenta boxes filled with a standard hydroponic solution of 1.25 mM KNO_3 , 0.75 mM MgSO_4 , 1.5 mM $\text{Ca}(\text{NO}_3)_2$, 0.5 mM KH_2PO_4 , 50 μM FeEDTA, 50 μM H_3BO_3 , 12 μM MnSO_4 , 0.7 μM CuSO_4 , 1 μM ZnSO_4 , 0.24 μM MoO_4Na_2 , and 100 μM

Na_2SiO_3 with pH 5.7 (as described in Boursiac et al., 2010). Hydroponic solutions were changed once every week. For suppression conditions, the standard hydroponic solution was supplemented with an additional nutrient, as mentioned in the figure legend (Supplemental Figure S5).

T-DNA insertion alleles

The following T-DNA insertion alleles were used for disruption in *ACA1* (At1g27770): *aca1-7* (GABI_095C01; seed stock ss2202, sulfadiazine resistant (Sulf^R)) and *aca1-2* (Wis_J789 alpha; ss28, kanamycin resistant (Kan^R)); *ACA2* (At4g37640): *aca2-2* (SAIL_873_F03; ss123, glufosinate resistant (Basta^R)), *aca2-3* (SALK_082624; ss493, Kan^R), and *aca2-5* (GABI_458B03; ss2257, Sulf^R); *ACA7* (At2g22950): *aca7-5* (SALK_132552; ss627, Kan^R), *aca7-8* (GABI_452E05; ss2207, Sulf^R), *aca7-9* (Wis_J3281 alpha; ss49, Kan^R), and *aca7-10* (SALK_014124; ss157, Kan^R). All T-DNA insertion alleles were in the wild-type Col-0 ecotype except for *aca1-2* and *aca7-9*, which were in the WS ecotype (Krysan et al., 1996). The position of T-DNA insertions and primers used for genotyping PCR are shown in Supplemental Figure S3. Primer sequences are shown in Supplemental Table S2. The two triple KO combinations created were *aca1-7/2-3/7-5* (ss1854) and *aca1-2/2-2/7-9* (ss1853).

Plasmid construction

For plant expression, all clones were constructed using standard molecular techniques using a pGreenII vector system (Hellens et al., 2000) with a Kan^R selection marker for bacteria, and a hygromycin resistance (Hyg^R) selection marker for plants, except where noted for ps396, which has a Kan^R for plant expression. ACAs were PCR amplified and cloned as full-length cDNA or genomic DNAs. All PCR products were sequenced to verify the absence of errors. Promoters used included a broadly expressed 35S promoter from *Cauliflower mosaic virus* (Benfey and Chua, 1990), a pollen-preferred promoter upstream from *ACA9* (Schiøtt et al., 2004), a native *ACA7* promoter sequence, and a *Ubiquitin 10* promoter (*UBQ10*; Norris et al., 1993).

The plasmid sequences are provided in Supplemental File S1 for plasmid stocks (ps) 35S::GFP (ps346), 35S::ACA8-GFP (ps396, with Kan^R), 35S::ACA2-GFP (ps660), 35S::ACA1-YFP (ps1294), 35S::ACA7-YFP (ps2091), *UBQ10::ACA7-YFP-Halo* (ps2682), 35S::YC-Nano65 (ps2151), *ACA9::ACA1-YFP* (ps1295), *ACA9::ACA2-GFP* (ps585), *ACA9::ACA7-YFP* (ps1960), *ACA9::ACA9-YFP* (ps580), *ACA9::YFP* (ps532), and *ACA7::ACA7-YFP* (ps2049).

For expression of YC-Nano65 in *E. coli*, the YC-nano65 insert was subcloned from a plant expression vector (ps2151) to a pET28-Novagen vector (Sigma-Aldrich) and named ps2966, *pET28-YC-Nano65* (sequence provided in Supplemental File S1).

Plant transformation and the resulting transgenic lines

Plasmid constructs were transformed into *Agrobacterium tumefaciens* GV3101 with a *pSOUP* helper plasmid (Hellens

et al., 2000). Plant transformations were conducted using the floral dip method (Clough and Bent, 1998). Transgenic plants were selected for Hyg^R (25 mg/L), or Kan^R (50 mg/L). Transgenic lines with seed stock identification numbers are indicated in Figure legends.

Qualitative-PCR and RT-qPCR

Total RNA was isolated from Arabidopsis seedlings, rosette leaves, or mature pollen using the RNeasy Plant Mini Kit (Qiagen). RNA samples were cleaned at least twice using RNase-free DNase (Qiagen) to remove genomic DNA contamination. One microgram samples of total RNA were used for a reverse transcriptase reaction using iScript cDNA Synthesis Kit (Catalog #170-8891; Bio-Rad).

For qualitative PCR comparisons of *ACA1*, 2, and 7 expressions in homozygous T-DNA mutants, a sample of 0.15 μ g of cDNA was used in a PCR reaction using DNA Taq polymerase (Catalog #M0273L; New England Biology) following the manufacturer's instructions. *ACA1*, 2, and 7 were amplified using primers indicated in Supplemental Table S2. *Actin 7* (At5g09810) was used as a housekeeping gene. The PCR products were analyzed on 2% (w/v) agarose gels and stained with ethidium bromide.

For real-time quantitative PCR (RT-qPCR), 0.15 μ g of cDNA was used in the real-time PCR reaction. For Taqman assays, SsoFast Probes Supermix (Catalog #172-5231; Bio-Rad) was used following the manufacturer's instructions. Taqman assays used in this study included *EF1- α* (*ef1-alpha*, AT5G60390), *PR1* (AT2G14610), *FRK1* (AT2G19190), and *PHI1* (AT1G35140) with assay ID numbers At02337969_g1, At02170748_s1, At02177526_g1, and At02193814_s1, respectively, from Applied Biosystems. For *PR2* (AT3G57260), SsoAdvanced Universal SYBR Green Supermix (Catalog #172-5271; Bio-Rad) was used according to manufacturer's instructions. The list of oligo sequences used in SYBR Green assays is shown in Supplemental Table S2. Primers for *PR2* were based on (Kaurilind and Brosché, 2017), and *EF1- α* was used for normalization in both methods (Lilly et al., 2011). Gene expression levels were quantified by RT-qPCR using a thermocycler CFX96 (Bio-Rad). The PCR conditions were as follows: 2 min at 95°C, 39 cycles of 95°C for 15 s and 1 min at 60°C. The $\Delta\Delta$ Ct method was used for data normalization (Livak and Schmittgen, 2001).

In vitro pollen germination

Pollen from the open flowers (stages 13 and 14) were transferred to glass slides with a layer of pollen germination media consisting of 0.8 mM MES, 1 mM KCl, 9 mM CaCl₂, 1 mM Ca(NO₃)₂, 0.8 mM MgSO₄, 1.5 mM H₃BO₃, 16.6% (w/v) sucrose (Fan et al., 2001), and 1% (w/v) low melting agar. The slides were then placed in square plates containing a wet Kim Wipe to maintain humidity. Pollen tubes were grown at room temperature in the dark for 3 h.

Seed set analyses

For seed set analyses, 10 consecutive siliques were harvested from the primary bolt. Siliques were decolorized by

incubating in 70% ethanol for 24 h at 22°C. Four individual plants were used for each genotype. The cleared siliques were then scanned into images used for seed counting.

Confocal microscopy

Confocal microscopy images were taken using an Olympus IX81 FV1000 confocal microscope equipped with the Olympus FluoView 1.07.03.00 software package (Olympus, Center Valley, PA, USA). For all images, a 60 \times objective (numerical aperture 1.42) was used. Excitation (ex) at wavelengths of 488 nm (GFP), 515 nm (YFP), and 543 nm (chlorophyll autofluorescence) were provided using an argon-ion or HeNe laser. A spectral emission (em) range of 500–545 nm for GFP, 530–570 nm for YFP, and 687–787 nm for chlorophyll autofluorescence was used.

Calcium imaging

For FRET-YFP/CFP ratio imaging, wild-type or *aca1/2/7* seedlings expressing YC-Nano65 were germinated and grown in petri dishes with 1/2x Epstein growth medium containing 0.1% (w/v) sucrose, 0.5% (w/v) Phytigel (pH 5.7; Lim et al., 2019) for 7 d in the growth chamber under long day photoperiod (16-h light/8-h dark) at 23°C/21°C (day/night) under cool white fluorescent lights (120 μ mol m⁻² s⁻¹). Images were collected using an AxioZoom V16 fluorescent microscope with a PlanNeoFluar Z 1.0x/0.25x objective (Carl Zeiss, Inc., Thornwood, NY, USA) and ORCA-Flash4.0 V2 Plus sCMOS digital camera (Hamamatsu Photonics Inc., San Jose, CA, USA). YC-Nano65 signals were acquired by excitation with ex440/40 nm, 24 μ mol m⁻² s⁻¹ intensity light and emission detected using a 495 nm long pass (LP) dichroic mirror and filters for exCFP (475/20 nm) and cpVenus (FRET, em540/30 nm). For a blue-light response, plants were pre-adapted to dim light and imaging was initiated at the start of a continuous blue-light stimulus (ex440/40 nm, 24 μ mol m⁻² s⁻¹ intensity). For *flg22* elicitor-triggered responses, plants were pre-adapted to a continuous blue-light illumination condition for at least 1 h until the establishment of stable baseline FRET-YFP/CFP ratio. *Flg22* peptide (QRLSTGSRINSKDDAAGLQIA) was obtained from Phytotechnology Laboratories (Shawnee Mission, KS) and dissolved in water according to manufacturer's recommendation. To test for *flg22* response, a 2- μ L aliquot of a 500 nM *flg22* solution, or a mock water control, was pipetted into a 24-h-old pre-established wound site (see Figure 10). Ratio images of FRET-YFP/CFP were acquired every 2 s for the duration of the experiments.

For FRET-YFP/CFP ratio imaging of YC-Nano65 in *E. coli*, T7 Express cells (New England Biolabs) were transformed with ps2966, *pET28-YC-Nano65*, and selected for Kan^R. Cells were grown with 2xYT media (Sigma-Aldrich) and imaged as described in Supplemental Figure S6 on solid media solidified with 1% agar, or in suspension in liquid 2xYT.

Quantitative analysis of [Ca²⁺]_{cyt} response was performed using ImageJ software (<http://imagej.nih.gov/ij/>) for the calculation of FRET-YFP/CFP ratio for YC-Nano65. Briefly, two channel images were first split into single YFP (FRET signal)

and CFP (background signal) channel images. Using the image process function in ImageJ software, ratio images were generated by dividing YFP channel images by CFP channel images. The extracted quantitative ratio numerical data from the time course images were displayed as a line graph using GraphPad Prism 6 software (GraphPad, Inc., La Jolla, CA, USA).

Accession numbers

T-DNA insertion mutant lines used in the study are as follows: for *ACA1* (At1g27770) T-DNA mutants: *aca1-2* (Wis_J789 alpha) and *aca1-7* (GABI_095C01); for *ACA2* (At4g37640) T-DNA mutants: *aca2-2* (SAIL_873_F03), *aca2-3* (SALK_082624), and *aca2-5* (GABI_458B03); For *ACA7* (At2g22950) T-DNA mutants: *aca7-5* (SALK_132552), *aca7-8* (GABI_452E05), *aca7-9* (Wis_J3281 alpha), and *aca7-10* * (SALK_014124). **aca7-10* is equal to *aca7-1* in (Lucca and León, 2012). Sequence data from this manuscript are available at the Arabidopsis Genome Initiative database under the following accession numbers: *ACA1* (At1g27770), *ACA2* (At4g37640), *ACA7* (At2g22950).

Supplemental data

The following materials are available in the online version of this article.

Supplemental Figure S1. Imaging showing subcellular localization for *ACA1* and *ACA7*.

Supplemental Figure S2. Relative protein expression levels for *ACA1*-YFP and *ACA7*-YFP in independent transgenic lines used to test for a rescue of a PM *aca9* fertility defect.

Supplemental Figure S3. Gene models with primer locations used for genotyping and qualitative PCR analyses of mRNAs.

Supplemental Figure S4. Seedlings harboring an *aca1/2/7* triple KO show increased mRNA expression for markers associated with Ca^{2+} -dependent (*FRK1*, *PHI1*) and SA-dependent (*PR2*) defense responses.

Supplemental Figure S5. Nutritional supplements inhibit lesion formation in *aca1/2/7* triple KO plants grown in hydroponics.

Supplemental Figure S6. FRET Imaging of YC-Nano65 expressed in *E. coli* fails to show a blue-light triggered $[\text{Ca}^{2+}]_{\text{cyt}}$ response.

Supplemental Figure S7. Imaging of GCaMP6f fluorescence showing a blue-light-triggered $[\text{Ca}^{2+}]_{\text{cyt}}$ response in wild-type cotyledons similar to those observed by FRET-imaging of the YC-Nano65 reporter.

Supplemental Figure S8. FRET imaging of YC-Nano65 showing Ca^{2+} dynamics triggered by blue light are similar in cotyledons from *aca1/2/7* seedlings with or without a *NahG* transgene.

Supplemental Figure S9. FRET imaging of YC-Nano65 in wild-type leaves showing Ca^{2+} transients are triggered by a flg22 pathogen elicitor but not a mock control.

Supplemental File S1. DNA sequences of plasmid constructs.

Supplemental Table S1. Comparison of published expression profiles for P-type ATPases in selected tissues.

Supplemental Table S2. List of primer sequences used for genotyping, cloning, qualitative PCR, and RT-qPCR.

Supplemental Movie S1. Imaging of *ACA1*-YFP in pollen showing streaming of ER-like strands.

Supplemental Movie S2. Imaging of blue light-triggered Ca^{2+} transients in wild-type and *aca1/2/7* KO plants.

Acknowledgment

We would like to thank Chrystle Weigand for technical assistance in RT-qPCR, and Su-Hwa Kim for assistance in Ca^{2+} imaging.

Funding

This work was supported by the United States Department of Agriculture (HATCH grant no. NEV00384 to J.F.H.), the National Science Foundation (IOS grant no. 1656774 to J.F.H., and MCB grant no. 2016143 to WC), US-Israel Binational Agricultural Research and Development Fund (BARD grant no. IS-4652-13 to J.F.H.), and the National Institute of General Medical Sciences of the National Institutes of Health (grant no. P20 GM103554 for microscopy).

Conflict of interest statement. None declared.

References

- Aldon D, Mbengue M, Mazars C, Galaud JP (2018) Calcium signaling in plant biotic interactions. *Int J Mol Sci* **19**: 665–684
- Alonso JM, Stepanova AN, Lisse TJ, Kim CJ, Chen H, Shinn P, Stevenson DK, Zimmerman J, Barajas P, Cheuk R, et al. (2003) Genome-wide insertional mutagenesis of *Arabidopsis thaliana*. *Science* **301**: 653–657
- Astegno A, Bonza MC, Vallone R, La Verde V, D’Onofrio M, Luoni L, Molesini B, Dominici P (2017) *Arabidopsis* calmodulin-like protein CML36 is a calcium (Ca^{2+}) sensor that interacts with the plasma membrane Ca^{2+} -ATPase isoform *ACA8* and stimulates its activity. *J Biol Chem* **292**: 15049–15061
- Axelsen KB, Palmgren MG (2001) Inventory of the superfamily of P-type ion pumps in *Arabidopsis*. *Plant Physiol* **126**: 696–706
- Badura A, Sun XR, Giovannucci A, Lynch LA, Wang SS-H (2014) Fast calcium sensor proteins for monitoring neural activity. *Neurophotonics* **1**: 025008-1–11
- Baum G, Long JC, Jenkins GI, Trewavas AJ (1999) Stimulation of the blue light phototropic receptor NPH1 causes a transient increase in cytosolic Ca^{2+} . *Proc Natl Acad Sci U S A* **96**: 13554–13559
- Baxter I, Tchieu J, Sussman MR, Boutry M, Palmgren MG, Gribskov M, Harper JF, Axelsen KB (2003) Genomic comparison of P-type ATPase ion pumps in *Arabidopsis* and rice. *Plant Physiol* **132**: 618–628
- Benfey PN, Chua NH (1990) The cauliflower mosaic virus 35S promoter: combinatorial regulation of transcription in plants. *Science* **250**: 959–966
- Boudsocq M, Willmann MR, McCormack M, Lee H, Shan L, He P, Bush J, Cheng SH, Sheen J (2010) Differential innate immune signalling via Ca^{2+} sensor protein kinases. *Nature* **464**: 418–422
- Boursiac Y, Harper JF (2007) The origin and function of calmodulin regulated Ca^{2+} pumps in plants. *J Bioenerg Biomembr* **39**: 409–414

- Boursiac Y, Lee SM, Romanowsky S, Blank R, Sladek C, Chung WS, Harper JF** (2010) Disruption of the vacuolar calcium-ATPases in Arabidopsis results in the activation of a salicylic acid-dependent programmed cell death pathway. *Plant Physiol* **154**: 1158–1171
- Bruiggeman Q, Raynaud C, Benhamed M, Delarue M** (2015) To die or not to die? Lessons from lesion mimic mutants. *Front Plant Sci* **6**: 1–22
- Choi W-G, Toyota M, Kim S-H, Hilleary R, Gilroy S** (2014) Salt stress-induced Ca^{2+} waves are associated with rapid, long-distance root-to-shoot signaling in plants. *Proc Natl Acad Sci USA* **111**: 6497–6502
- Clough SJ, Bent AF** (1998) Floral dip: a simplified method for Agrobacterium-mediated transformation of *Arabidopsis thaliana*. *Plant J* **16**: 735–743
- Costa A, Luoni L, Marrano CA, Hashimoto K, Köster P, Giacometti S, De Michelis MI, Kudla J, Bonza MC** (2017) Ca^{2+} -dependent phosphoregulation of the plasma membrane Ca^{2+} -ATPase ACA8 modulates stimulus-induced calcium signatures. *J Exp Bot* **68**: 3215–3230
- Delaney TP, Uknes S, Vernooij B, Friedrich L, Weymann K, Negrotto D, Gaffney T, Gut-Rella M, Kessmann H, Ward E, et al.** (1994) A central role of salicylic acid in plant disease resistance. *Science* **266**: 1247–1250
- Demidchik V, Shabala S, Isayenkov S, Cuin TA, Pottosin I** (2018) Calcium transport across plant membranes: mechanisms and functions. *New Phytol* **220**: 49–69
- dit Frey NF, Mbengue M, Kwaaitaal M, Nitsch L, Altenbach D, Häwker H, Lozano-Duran R, Njo MF, Beeckman T, Huettel B, et al.** (2012) Plasma membrane calcium ATPases are important components of receptor-mediated signaling in plant immune responses and development. *Plant Physiol* **159**: 798–809
- Du L, Ali GS, Simons KA, Hou J, Yang T, Reddy ASN, Poovaiah BW** (2009) Ca^{2+} /calmodulin regulates salicylic-acid-mediated plant immunity. *Nature* **457**: 1154–1158
- Dunkley TPJ, Hester S, Shadforth IP, Runions J, Weimar T, Hanton SL, Griffin JL, Bessant C, Brandizzi F, Hawes C, et al.** (2006) Mapping the *Arabidopsis* organelle proteome. *Proc Natl Acad Sci U S A* **103**: 6518–6523
- Fan LM, Wang YF, Wang H, Wu WH** (2001) In vitro *Arabidopsis* pollen germination and characterization of the inward potassium currents in *Arabidopsis* pollen grain protoplasts. *J Exp Bot* **52**: 1603–1614
- Fromm H, Finkler A** (2015) Repression and de-repression of gene expression in the plant immune response: the complexity of modulation by Ca^{2+} and calmodulin. *Mol Plant* **8**: 671–673
- Gaffney T, Friedrich L, Vernooij B, Negrotto D, Nye G, Uknes S, Ward E, Kessmann H, Ryals J** (1993) Requirement of salicylic acid for the induction of systemic acquired resistance. *Science* **261**: 754–756
- García Bossi J, Kumar K, Barberini ML, Domínguez GD, Rondón Guerrero YDC, Marino-Buslje C, Obertello M, Muschiatti JP, Estevez JM** (2020) The role of P-type IIA and P-type IIB Ca^{2+} -ATPases in plant development and growth. *J Exp Bot* **71**: 1239–1248
- George L, Romanowsky SM, Harper JF, Sharrock RA** (2008) The ACA10 Ca^{2+} -ATPase regulates adult vegetative development and inflorescence architecture in Arabidopsis. *Plant Physiol* **146**: 716–728
- Giacometti S, Marrano CA, Bonza MC, Luoni L, Limonta M, De Michelis MI** (2012) Phosphorylation of serine residues in the N-terminus modulates the activity of ACA8, a plasma membrane Ca^{2+} -ATPase of *Arabidopsis thaliana*. *J Exp Bot* **63**: 1215–1224
- Harada A, Sakai T, Okada K** (2003) phot1 and phot2 mediate blue light-induced transient increases in cytosolic Ca^{2+} differently in *Arabidopsis* leaves. *Proc Natl Acad Sci U S A* **100**: 8583–8588
- Harada A, Shimazaki K** (2007) Phototropins and blue light-dependent calcium signaling in higher plants. *Photochem Photobiol* **83**: 102–111
- Harper JF, Hong B, Hwang I, Guo HQ, Stoddard R, Huang JF, Palmgren MG, Sze H** (1998) A novel calmodulin-regulated Ca^{2+} -ATPase (ACA2) from *Arabidopsis* with an N-terminal autoinhibitory domain. *J Biol Chem* **273**: 1099–1106
- Hellens RP, Edwards EA, Leyland NR, Bean S, Mullineaux PM** (2000) pGreen: a versatile and flexible binary Ti vector for Agrobacterium-mediated plant transformation. *Plant Mol Biol* **42**: 819–832
- Hilleary R, Paez-Valencia J, Vens C, Toyota M, Palmgren M, Gilroy S** (2020) Tonoplast-localized Ca^{2+} pumps regulate Ca^{2+} signals during pattern-triggered immunity in *Arabidopsis thaliana*. *Proc Natl Acad Sci U S A* **117**: 18849–18857
- Himschoot E, Pleskot R, Van Damme D, Vanneste S** (2017) The ins and outs of Ca^{2+} in plant endomembrane trafficking. *Curr Opin Plant Biol* **40**: 131–137
- Hocking B, Conn SJ, Manohar M, Xu B, Athman A, Stancombe MA, Webb AR, Hirschi KD, Gilliam M** (2017) Heterodimerization of *Arabidopsis* calcium/proton exchangers contributes to regulation of guard cell dynamics and plant defense responses. *J Exp Bot* **68**: 4171–4183
- Hong B, Ichida A, Wang Y, Gens JS, Pickard BG, Harper JF** (1999) Identification of a calmodulin-regulated Ca^{2+} -ATPase in the endoplasmic reticulum. *Plant Physiol* **119**: 1165–1175
- Huang L, Berkelman T, Franklin AE, Hoffman NE** (1993) Characterization of a gene encoding a Ca^{2+} -ATPase-like protein in the plastid envelope. *Proc Natl Acad Sci U S A* **90**: 10066–10070
- Hwang I, Sze H, Harper JF** (2000) A calcium-dependent protein kinase can inhibit a calmodulin-stimulated Ca^{2+} pump (ACA2) located in the endoplasmic reticulum of *Arabidopsis*. *Proc Natl Acad Sci U S A* **97**: 6224–6229
- Iino M** (1988) Desensitization by red and blue light of phototropism in maize coleoptiles. *Planta* **176**: 183–188
- Iwano M, Igarashi M, Tarutani Y, Kaothien-Nakayama P, Nakayama H, Moriyama H, Yakabe R, Entani T, Shimosato-Asano H, Ueki M, et al.** (2014) A pollen coat-inducible autoinhibited Ca^{2+} -ATPase expressed in stigmatic papilla cells is required for compatible pollination in the Brassicaceae. *Plant Cell* **26**: 636–649
- Janoudi AK, Poff KL** (1991) Characterization of adaptation in phototropism of *Arabidopsis thaliana*. *Plant Physiol* **95**: 517–521
- Janoudi AK, Poff KL** (1993) Desensitization and recovery of phototropic responsiveness in *Arabidopsis thaliana*. *Plant Physiol* **101**: 1175–1180
- Johnson MA, Harper JF, Palanivelu R** (2019) A fruitful journey: pollen tube navigation from germination to fertilization. *Annu Rev Plant Biol* **70**: 809–837
- Kaurilind E, Brosché M** (2017) Stress marker signatures in lesion mimic single and double mutants identify a crucial leaf age-dependent salicylic acid related defense signal. *PLoS One* **12**: e0170532 doi: 10.1371/journal.pone.0170532
- Kim Y-Y, Choi H, Segami S, Cho H-T, Martinoia E, Maeshima M, Lee Y** (2009) AtHMA1 contributes to the detoxification of excess Zn(II) in *Arabidopsis*. *Plant J* **58**: 737–753
- Klessig DF, Choi HW, Dempsey DA** (2018) Systemic acquired resistance and salicylic acid: past, present, and future. *Mol Plant-Microbe Interact* **31**: 871–888
- Krysan PJ, Young JC, Tax F, Sussman MR** (1996) Identification of transferred DNA insertions within *Arabidopsis* genes involved in signal transduction and ion transport. *Proc Natl Acad Sci U S A* **93**: 8145–8150
- Kudla J, Becker D, Grill E, Hedrich R, Hippler M, Kummer U, Parniske M, Romeis T, Schumacher K** (2018) Advances and current challenges in calcium signaling. *New Phytol* **218**: 414–431
- Lee SM, Kim HS, Han HJ, Moon BC, Kim CY, Harper JF, Chung WS** (2007) Identification of a calmodulin-regulated autoinhibited Ca^{2+} -ATPase (ACA11) that is localized to vacuole membranes in *Arabidopsis*. *FEBS Lett* **581**: 3943–3949
- Li Y, Guo J, Yang Z, Yang DL** (2018) Plasma membrane-localized calcium pumps and copines coordinately regulate pollen germination and fertility in Arabidopsis. *Int J Mol Sci* **19**: 1774–1780

- Lilly ST, Drummond RSM, Pearson MN, MacDiarmid RM** (2011) Identification and validation of reference genes for normalization of transcripts from virus-infected *Arabidopsis thaliana*. *Mol Plant-Microbe Interact* **24**: 294–304
- Lim SD, Kim SH, Gilroy S, Cushman JC, Choi WG** (2019) Quantitative ROS bioreporters: a robust toolkit for studying biological roles of ROS in response to abiotic and biotic stresses. *Physiol Plant* **165**: 356–368
- Limonta M, Romanowsky S, Olivari, Bonza MC, Luoni L, Rosenberg A, Harper JF, De Michelis MI** (2014) ACA12 is deregulated isoform of plasma membrane Ca^{2+} -ATPase of *Arabidopsis thaliana*. *Plant Mol Biol* **84**(4–5): 387–397
- Livak KJ, Schmittgen TD** (2001) Analysis of relative gene expression data using real-time quantitative PCR and the $2^{-\Delta\Delta\text{CT}}$ method. *Methods* **25**: 402–408
- Lopreiato R, Giacomello M, Carafoli E** (2014) The plasma membrane calcium pump: new ways to look at an old enzyme. *J Biol Chem* **289**: 10261–10268
- Lucca N, León G** (2012) *Arabidopsis* ACA7, encoding a putative auto-regulated Ca^{2+} -ATPase, is required for normal pollen development. *Plant Cell Rep* **31**: 651–659
- Luria G, Rutley N, Lazar I, Harper JF, Miller G** (2019) Direct analysis of pollen fitness by flow cytometry: implications for pollen response to stress. *Plant J* **98**: 942–952
- Ma Y, Berkowitz GA** (2017) Multimeric CAX complexes and Ca^{2+} signaling – Beyond humdrum housekeeping. *J Exp Bot* **68**: 3997–3999
- Malmström S, Askerlund P, Palmgren MG** (1997) A calmodulin-stimulated Ca^{2+} -ATPase from plant vacuolar membranes with a putative regulatory domain at its N-terminus. *FEBS Lett* **400**: 324–328
- Martí Ruiz MC, Jung HJ, Webb AAR** (2020) Circadian gating of dark-induced increases in chloroplast- and cytosolic-free calcium in *Arabidopsis*. *New Phytol* **225**: 1993–2005
- Miché L, Battistoni F, Gemmer S, Belghazi M, Reinhold-Hurek B** (2018) Host-dependent expression of *Rhizobium leguminosarum* bv. *viciae* hydrogenase is controlled at transcriptional and post-transcriptional levels in legume nodules. *Mol Plant-Microbe Interact* **19**: 1165–1174
- Moeder W, Phan V, Yoshioka K** (2019) Ca^{2+} to the rescue – Ca^{2+} channels and signaling in plant immunity. *Plant Sci* **279**: 19–26
- Molina A, Hunt MD, Ryals JA** (1998) Impaired fungicide activity in plants blocked in disease resistance signal transduction. *Plant Cell* **10**: 1903–1914
- Moore I, Murphy A** (2009) Validating the location of fluorescent protein fusions in the endomembrane system. *Plant Cell* **21**: 1632–1636
- Moreno I, Norambuena L, Maturana D, Toro M, Vergara C, Orellana A, Zurita-Silva A, Ordenes VR** (2008) AtHMA1 is a thapsigargin-sensitive Ca^{2+} /Heavy Metal Pump. *J Biol Chem* **283**: 9633–9641
- Norris SR, Meyer SE, Callis J** (1993) The intron of *Arabidopsis thaliana* polyubiquitin genes is conserved in location and is a quantitative determinant of chimeric gene expression. *Plant Mol Biol* **21**: 895–906
- Obermeyer G, Feijó J** (eds) (2017) *Pollen Tip Growth: from Biophysical Aspects to Systems Biology*. Springer International Publishing
- Palmer IA, Chen H, Chen J, Chang M, Li M, Liu F, Fu ZQ** (2019) Novel salicylic acid analogs induce a potent defense response in *Arabidopsis*. *Int J Mol Sci* **20**: 3356
- Pedersen CNS, Axelsen KB, Harper JF, Palmgren MG** (2012) Evolution of plant P-type ATPases. *Front Plant Sci* **3**: 31
- Pittman JK, Hirschi KD** (2016) CAX-ing a wide net: Cation/H⁺ + transporters in metal remediation and abiotic stress signalling. *Plant Biol* **18**: 741–749
- Pooaiah BW, Du L, Wang H, Yang T** (2013) Recent advances in calcium/calmodulin-mediated signaling with an emphasis on plant-microbe interactions. *Plant Physiol* **163**: 531–542
- Radojčić A, Li X, Zhang Y** (2018) Salicylic acid: a double-edged sword for programmed cell death in plants. *Front Plant Sci* **9**: 1133
- Rosso MG, Li Y, Strizhov N, Reiss B, Dekker K, Weisshaar B** (2003) An *Arabidopsis thaliana* T-DNA mutagenized population (GABI-Kat) for flanking sequence tag-based reverse genetics. *Plant Mol Biol* **53**(1–2): 247–259
- Sanchez SE, Rugnone ML, Kay SA** (2020) Light perception: a matter of time. *Mol Plant* **13**: 363–385
- Schiøtt M, Romanowsky SM, Bækgaard L, Jakobsen MK, Palmgren MG, Harper JF** (2004) A plant plasma membrane Ca^{2+} pump is required for normal pollen tube growth and fertilization. *Proc Natl Acad Sci U S A* **101**: 9502–9507
- Seigneurin-Berny D, Gravot A, Auroy P, Mazard C, Kraut A, Finazzi G, Grunwald D, Rappaport F, Vavasseur A, Joyard J, et al.** (2006) HMA1, a new Cu-ATPase of the chloro plast envelope, is essential for growth under adverse light conditions. *J Biol Chem* **281**: 2882–2892
- Sessions A, Burke E, Presting G, Aux G, McElver J, Patton D, Dietrich B, Ho P, Bacwaden J, Ko C, et al.** (2002) A high-throughput *Arabidopsis* reverse genetics system. *Plant Cell* **14**: 2985–2994
- Seyfferth C, Tsuda K** (2014) Salicylic acid signal transduction: the initiation of biosynthesis, perception and transcriptional reprogramming. *Front Plant Sci* **5**: 697
- Spalding EP, Harper JF** (2011) The ins and outs of cellular Ca^{2+} transport. *Curr Opin Plant Biol* **14**: 715–720
- Stone LM, Seaton KA, Kuo J, McComb JA** (2004) Fast pollen tube growth in *Conospermum* species. *Ann Bot* **93**: 369–378
- Sun W, Dunning FM, Pfund C, Weingarten R, Bent AF** (2006) Within-species flagellin polymorphism in *Xanthomonas campestris* pv. *campestris* and its impact on elicitation of *Arabidopsis* FLAGELLIN SENSING2-dependent defenses. *Plant Cell* **18**: 764–779
- Tang RJ, Luan S** (2017) Regulation of calcium and magnesium homeostasis in plants: from transporters to signaling network. *Curr Opin Plant Biol* **39**: 97–105
- Tena G** (2019) Flagellin unmasked. *Nat Plants* **5**: 452
- Truman W, Sreekanta S, Lu Y, Bethke G, Tsuda K, Katagiri F, Glazebrook J** (2013) The CALMODULIN-BINDING PROTEIN60 family includes both negative and positive regulators of plant immunity. *Plant Physiol* **163**: 1741–1751
- Wang L, Tsuda K, Sato M, Cohen JD, Katagiri F** (2009) *Arabidopsis* CaM binding protein CBP60g contributes to MAMP-induced SA accumulation and is involved in disease resistance against *Pseudomonas syringae*. *PLoS Pathog* **5**: 1000301
- Wang Q, Jiang M, Isupov MN, Chen Y, Littlechild JA, Sun L, Wu X, Wang Q, Yang W, Chen L, et al.** (2020) The crystal structure of *Arabidopsis* BON1 provides insights into the copine protein family. *Plant J* **103**: 1215–1232
- Woody ST, Austin-Phillips S, Amasino RM, Krysan PJ** (2007) The WiscDsLox T-DNA collection: an *Arabidopsis* community resource generated by using an improved high-throughput T-DNA sequencing pipeline. *J Plant Res* **120**: 157–165
- Yang DL, Shi Z, Bao Y, Yan J, Yang Z, Yu H, Li Y, Gou M, Wang S, Zou B, et al.** (2017) Calcium pumps and interacting BON1 protein modulate calcium signature, stomatal closure, and plant immunity. *Plant Physiol* **175**: 424–437
- You IS, Ghosal D, Gunsalus IC** (1991) Nucleotide sequence analysis of the *Pseudomonas putida* PpG7 salicylate hydroxylase gene (*nahG*) and its 3'-flanking region. *Biochemistry* **30**: 1635–1641
- Yu H, Yan J, Du X, Hua J** (2018) Overlapping and differential roles of plasma membrane calcium ATPases in *Arabidopsis* growth and environmental responses. *J Exp Bot* **69**: 2693–2703
- Zhang J, Zhang X, Wang R, Li W** (2014) The plasma membrane-localised Ca^{2+} -ATPase ACA8 plays a role in sucrose signalling involved in early seedling development in *Arabidopsis*. *Plant Cell Rep* **33**: 755–766

Zhao X, Wang YL, Qiao XR, Wang J, Wang LD, Xu CS, Zhang X (2013) Phototropins function in high-intensity blue light-induced hypocotyl phototropism in arabidopsis by altering cytosolic calcium. *Plant Physiol* **162**: 1539–1551

Zhu X, Caplan J, Mamillapalli P, Czymbek K, Dinesh-Kumar SP (2010) Function of endoplasmic reticulum calcium ATPase in innate immunity-mediated programmed cell death. *EMBO J* **29**: 1007–1018